A Study of Laser Cladding Deposition on Stainless Steel Alloys

Supervisors

Mihail Botan

David Busquets Mataix

Daniel-Eugeniu Crunteanu

Student:

Juan Carlos Campaña Cuenca

30/06/2022

Contents

Page

List of Figures

Page

List of Tables

Page

Aim

The aim of this study is develop a Laser Cladding deposition method suitable for stainless steel 304[1] as base material, and MetcoAdd 316L-D[2] as clad material.

The study will focus on tweaking and varying the different parameters in the deposition to achieve a consistent geometry, paying attention to avoid the formations of cracks in the surface, as well as analyzing the thermal affected zone and microstructure of the clad material via microscopy and microhardness test on the surface.

CHAPTER 1

Theoretical Background

1.1 Laser Deposition with Laser Cladding

[3][4][5][6][7]

Laser Beams provide a well controlled heat source, both in power delivery and in the spacial precision of the directed energy. This kind of interactions between the laser beam and the material are very different from other thermal processing methods such as plasma spray, arc, etc. This provides several advantages over competing processing methods used for thermal deposition.

There are lots of variations of the process that use a vast selection of lasers, material delivery, motion and control systems, each one optimized for a specific application.

Cladding is defined as the deposition of weld material on metallic substrates. Laser Cladding is fundamentally a type of coating technology that uses a focused or defocused high-power laser beam to locally melt the thin surface layer of a substrate and the added materials while at the same time forming a new layer of material with the desired properties after solidification. It is then, a process used to improve the superficial properties of an alloy, it is very useful in situations like highly corrosive environments such as the blade of a turbine, or to improve the wearing resistance. The deposited material forms a coating on the substrate, altering the surface properties, providing a combination of properties not achievable by other means. Usually, a base metal is selected with cost or structural properties in mind, while another metal is added for surface protection or any other desired property, such as electrical conductivity.

This technology provides with a large coverage area by overlapping individual tracks. The melting of the substrate is controlled so it is only enough to create a complete metallurgical bond at the interface, in this manner the dilution from the substrate is minimal, allowing the newly formed layer to retain the original composition and properties of the added materials.

The deposition involves the laser beam focusing on a small region, and the introduction of the clad material into the beam to fuse it with the substrate and form the coating.

There is a vast horizon of possibilities of power sources with wavelengths ranging between 1 and 10 μm. The movement of the laser relative to the part is controlled either from simple linear movements to complex CNC and programming techniques.

The main advantage of using lasers is that of reduced heat inputs, providing advantages such as geometric, precision of the deposit, economic (speed, material savings). Of course these advantages depends on the specific case keeping in mind that there is need for extra effort compared to more mature, more simple and more widely applied conventional alternatives.

Other coating technologies include thermal spray and plasma spray processes, but the thickness of their deposition is much lower and do not provide with a metallurgical bond between the clad and the substrate material due to the lack of fusion of the metals.

1.1.1 Process Description

Laser cladding technology uses a high energy density laser to deposit selected corrosion and wear resistant material on structural material substrates. The cladding materials (usually powders) normally have a very different physical properties (melting points, heat conductivity, etc.) from those of the substrates.

The lasers, due to being highly monochromatic and coherent with a high degree of directionality, are capable of being sharply focused, providing a power density in the order of 10^{17} W/cm^2, and can rapidly heat a metal surface to a temperature up to 10^5 K, which then rapidly cools at a rate up to 10^{6-7} K/s, so the melt remains for a short time, rapidly cooling and solidifying. Because of the high energy density that the laser provides it can be directed at a specific location of the substrate, resulting in a much lower heat input than it would be produced with an arc source. This is important because it minimizes the impact of the process on the substrate material, allowing it to be used both in thin and thick parts.

Due to the rapid heating, the phase transformation temperatures may increase dramatically, comparing with the ones presented in the equilibrium phase diagram. The melt pool can be stable and moving if it is produced by a continuous wave laser or last for a few microseconds, if it is produced by a pulse laser.

The temperature and temperature distributions depend on a number of design parameters of the process such as laser power density, beam spot size, traverse speed, powder flow rate and laser beam absorption.

The microstructure of the deposited layer is usually very fine, due to the rapid cooling, resulting in better metallurgical properties. Due to the high cooling rate, it also presents an increase in dislocation density and distortion of the

lattice. The solid solubility of the supersaturated solution increases significantly. Metastable phases or new phases can occur, due to the lack of diffusion. Rare earth elements often play an important role, modifying the melting and solidification processes. Laser cladding technology has demonstrated it is able to locally tailor the substrate surface to designed macro/microstructures with designed properties while maintaining the toughness and strength of the bulk substrates. It is also used for its 3D manufacturing capabilities.

The process produces a macrostructure similar to the ones obtained by arc-based processes, but providing smaller sizes for the working zones. In the Figure 1.1.1 it is possible to see the geometry of a laser clad. It includes the clad metal, a mixed zone between the substrate and the coating, a heat affected zone in the base material, and finally the base metal. These regions have different properties, with the clad material providing the seeked surface properties as it is stated above, and the mixed and heat affected zones resulting from the interaction of the heat source, the clad material and the substrate. The two last zones having small sizes due to the minimal impact of the process in the base material.

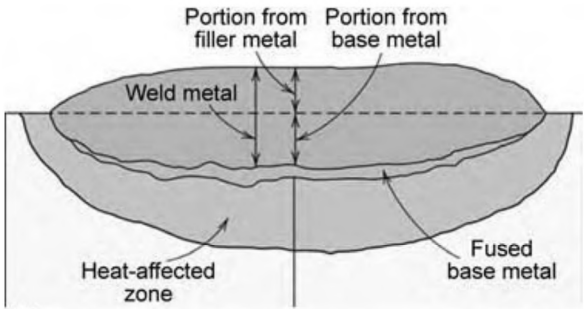

Figure 1.1.1: Schematic diagram of the the cross section of a Laser Cladding regions. Provided by Westinghouse Electric Company, WEC Welding Machining, LLC.

The microstructure of the different regions of the clad can be very different. In the Figure 3.3.1, it can be seen the gradient of grain size present in the clad.

Among other relevant applications of the process there are: repair of commercial aircraft and the application of corrosion, wear and oxidation resistant coatings on shafts of drilling tools, engine valve seats, tool hardfacing, hydraulic pump components and molds.[]

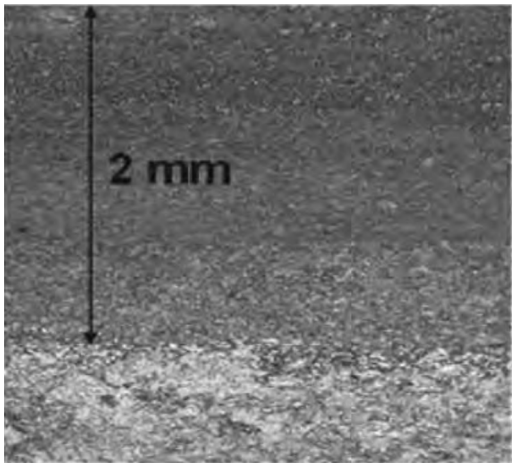

Figure 1.1.2: Gradient of grain size in the heat affected zone. Provided by Applied Research Laboratory, Pennsylvania State University.

1.1.2 Materials Combination

The possibilities of depositing corrosion and wear resistant materials on compatible substrate materials are huge. The case most relevant for this study is the deposition of these kind of materials on structural steel components, which is also the most common industrial application for this type of technology.[]

The coatings are usually cobalt base alloys for wear resistant coatings[]; nickel base alloys, such as Inconel for corrosion resistant applications; and iron base alloys, such as martensitic and austenitic stainless steels for both wear and corrosion applications.

The selection of the combination of base material and powder is driven by material compatibility and similar expansion coefficients between the two of them. Metallurgical compatibility is one of the primary considerations. Also, due to the fact that the clad and substrate will be fused, alloy combinations that will result in the formation of undesirable inter-metallic phases cannot be chosen. Nevertheless, as this method provides low level of base-metal dilution (particularly at low level heat inputs), the formation of this undesired phases can be limited.

1.1.3 The solidification process

This section discuss solidification-related phenomena regarding laser cladding, including rapid solidification (microstructual refinement, extended solid solution, metastable phases, amorphous structures) and directional solidification.

As it was mentioned earlier, the cooling rate in a laser cladding process has huge temperature gradients. This high cooling rate provides with very fine

solidification microstructures, and the existence of large coupled zones in eutectics. Solidification is directional, and the coatings are strongly textured as a consequence. The diffusion necessary to form transformation is supressed, but martensitic and massive non thermal transformation may occur. Extended solid solutions, metastable phases and even amorphous alloys can be observed.

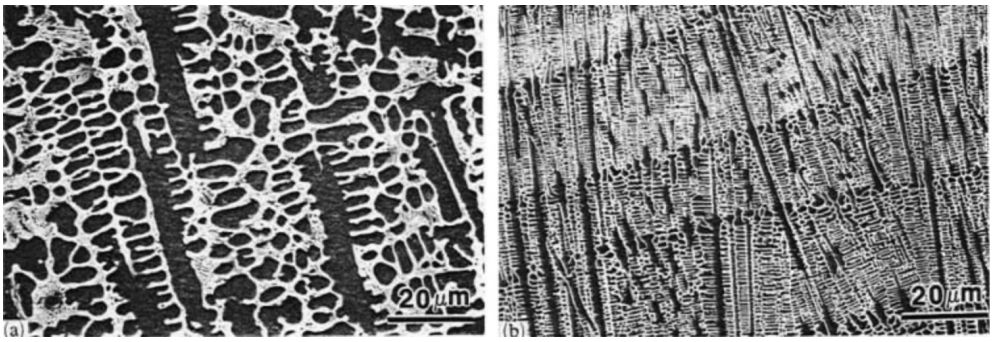

Figure 1.1.3: Cross section of Stellite 6 clad. The black dendritic phase corresponds to the cobalt-based matrix and the white is formed by M_7C_4 eutectic carbides. (a) Corresponds to a slow scanning speed of 1.67 mm/s and (b) to a high scanning speed of 167 mm/s.[]

There are three laser-deposited layers, in general. First a plane solidification front microstructure with limited thickness, then a transition cellular microstructure, and finally a columnar-dendritic microstructure. Under some conditions a fourth region consisting of uniaxed grains appears at the top. The microstructure of each section depends on the local solidification rate, the undercooling, and the temperature gradient.

This characteristic is very interesting in the aero-engine and gas turbine industries, where it is important to have columnar grain morphology, or even single crystal structures, aiming for an increase in the operating temperature of the turbines to improve overall efficiency.

1.1.4 Process Characteristics

Laser cladding is a flexible process in which a range of process parameters can be varied to produce a wide array of different coating thicknesses and process efficiencies. Several of these process parameter include laser power, beam diameter, travel speed, clad material-introduction mode and beam manipulation methods. The different combinations of these parameters have an impact on the type of materials deposited by the process, its efficiency (understood as the deposition rate of the clad material), the thickness of the coating and the impact on the substrate.

There are various methods of feeding the clad material. Mainly powder or wire feeding Figure 1.1.4. In both cases, the laser beam is directed at the powder or wire, then melted into the substrate surface. Each material introduction mode has unique properties, alongside their advantages and disadvantages. In this study powder feeding technique is used. The powder is fed into the melt pool by a delivery inert gas via a nozzle, passing through the laser beam absorbing some of the laser energy, and falling into the melt pool where it is fully melt and solidified. Some of the hardest particles may not completely melt, but they will partially dissolve.

When working with powder, it is possible to set a wide range of deposit rates each with its own characteristics. Low deposition rate allows for the laser clad layers to be produced with lower heat inputs, resulting in minimal distortion and allowing the deposition of thin clad layers. On the other hand, high deposition rate results in the deposition of thick clad layers on applications such as shafts or other components where there is a need for heavy protection against corrosion and wear conditions. However this technique has its limitations, its is tailored to specific geometries and welding positions, because some substrate configurations make it very difficult to place the powder.

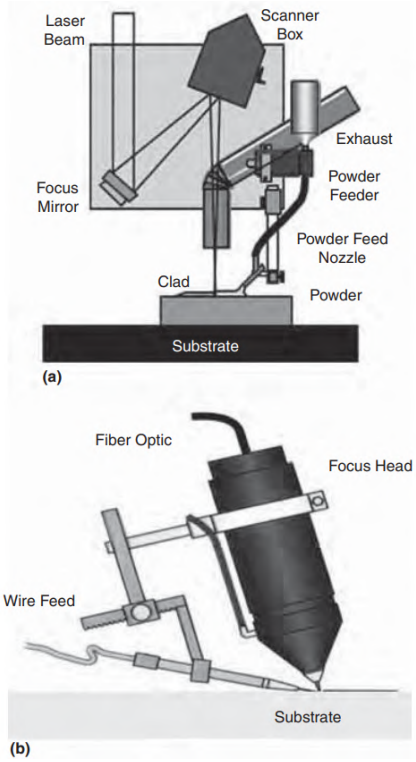

Figure 1.1.4: Schematic diagram of the (a) powder-fed and (b) wire-fed laser-cladding processes. Provided by Applied Research Laboratory, Pennsylvania State University

CHAPTER 2

Approach

2.1 Laser Deposition

In this section the procedure followed to obtain the final coating by laser cladding will be detailed. From the preparation of the samples to the tweaking of the machine parameters to obtain different characteristics in the coating.

2.1.1 Sand Blasting of the Samples

The samples are freshly cut, so they come out of the box with some dirt on the surface that need to be removed in order for the coating to attach in a better way to the part. This will be achieved via sandblasting the parts to clean them.

The sandblasting machine Figure 2.1.1 consist of a closed chamber, which can be accessed via gloves in the side, so all the powder is contained inside it. It is possible to look in the inside while working via a glass.

The abrasive particles are alumina powder, also known as Corundum. It is a very hard material, occupying the second place in the Mohs scale[8], only falling behind diamond.

The pistol has two tubes connected to it. One of them provides the pressured air, in this case 6 bars, and the other one provides the alumina powder. In this way it is possible to blast the samples and clean them. The corundum powder recirculates, as soon as it exits the pistol, it falls into the receptacle of the machine, which guides it back to the tube connected to the pistol.

In the figures 2.1.2a and 2.1.2b it can be seen the difference of the before and after the procedure, the surfaces are much more clean and polished.

Figure 2.1.1: Sand Blasting Machine

(a) (b)

Figure 2.1.2: Closeup of the before (a) and after (b) sandblasting

After this procedure, in order to eliminate any particle of alumina that may be on the surfaces first, the samples are cleaned with water and dried in a furnace at low temperature, around 60^{o}C (Figure 2.1.3).

Figure 2.1.3: Samples drying in the furnace

Then they are submerged in an alcoholic bath with ultrasounds for 30 minutes (Figure 2.1.4). After that, the samples are clean and ready to go receive the coating (Figure 2.1.5).

Figure 2.1.4: Ultrasounds Machine

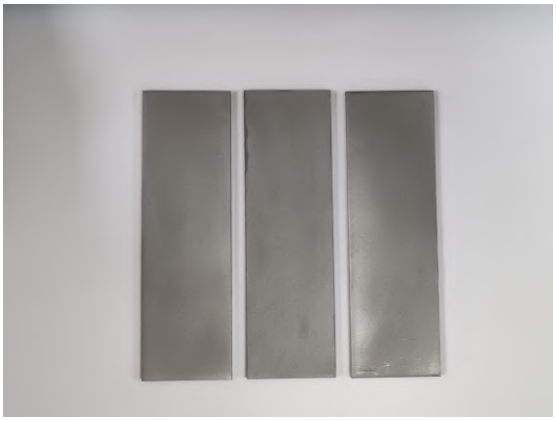

Figure 2.1.5: Samples after the ultrasonic bath

2.1.2 Laser Cladding

Once the samples are properly sanded and clean it is time to proceed to make the deposition.

Figure 2.1.6: Laser deposition machine

The laser equipment utilized is shown in Figure 2.1.6. It is an EVO CUBE from the company COHERENT. It is a closed workstation suitable for cladding, cutting and welding. The machine total working area is one cubic meter with a 3 axis gantry system, allowing a full CNC control.

It is a small cost-efficient system that allows high quality powder cladding with laser power up to 600W. The machine works with G-code.

In the Figure 2.1.7 there is a detail of the most important components of the laser cladding machine.

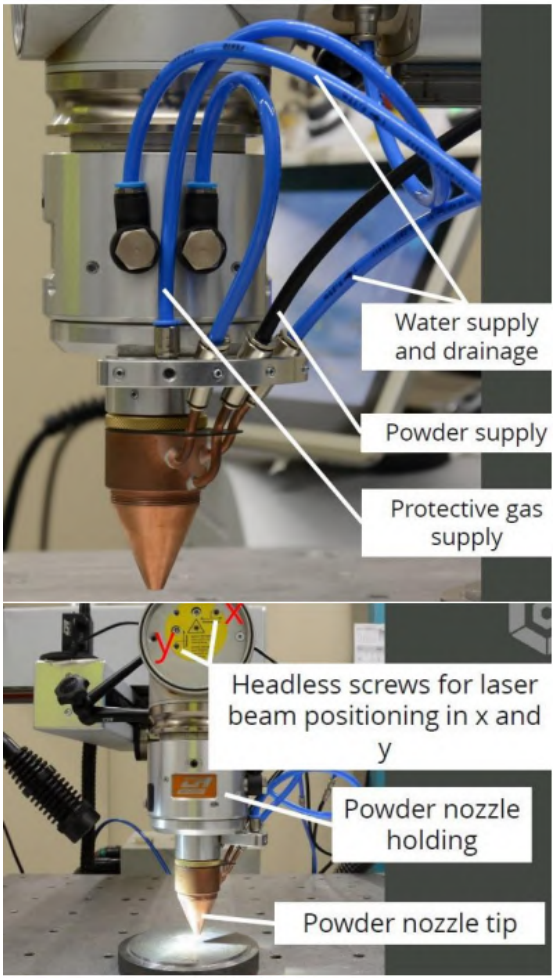

Figure 2.1.7: Main components of the EVO CUBE.

Positioning of the Laser

First of all there the need to position the laser so it is aligned properly with the test sample. It needs to be positioned in the XY plane, as well as in the Z axis. The part is fixed with screws into a thick plate so it does not move while the process is taking place.

For the Z axis, there is a positioner provided that is exactly 7 mm thick. The procedure is to put the sample underneath the laser beam, and the positioner on top of the test sample. Then, lower it until it barely touches the positioner. In that way it is guaranteed that the relative position of the laser and the part is correct. This positioning is important because it ensures that the laser is in focus, so it can work properly.

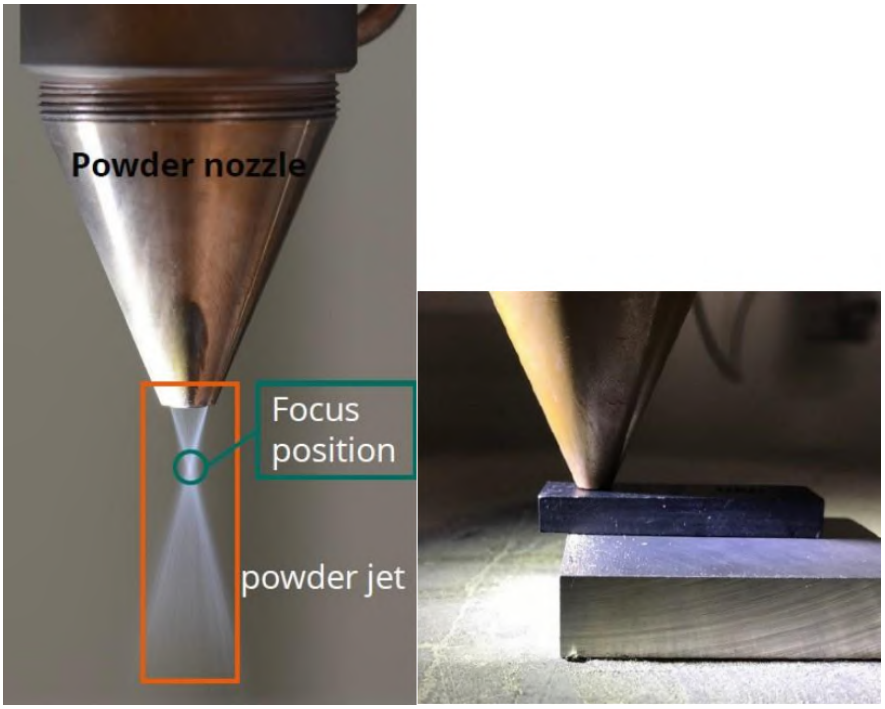

Figure 2.1.8: Positioning of the head of the laser machine in the Z axis.

The positioning in the XY plane is done manually. There is a function of the machine that allows to simulate the movement of the laser, but without any powder or actual power in it. This is useful to check that the path of the laser is always contained in the part.

Once this is checked it is possible to proceed to the actual deposition.

Power Test

First, a power test will be conducted. The goal is to study the geometry and crystallography produced in the test sample by each power level. This step is relevant because it will provide the height and width of the clad for each case, these parameters are crucial because they are required as input parameters in the software. This set of data can only be obtained experimentally, because it depends on the powder, the substrate and laser parameters. Once these values are known for each case, then it is possible to proceed to make depositions consisting of multiple layers.

The values of power studied are presented in the Table 2.1.1, The maximum power of the laser is 600W. The values of the test are presented in percentage of the full power and also in Watts.

Test	Power Level [%]	Power Level [W]
1	10	60
2	15	90
3	20	120
4	25	150
5	30	180
6	35	210
7	40	240
8	45	270
9	50	300
10	55	330
11	60	360
12	65	390
13	70	420
14	75	450

Table 2.1.1: Table showing the power levels of the laser tested, in percentage of the full power, and also in power

The gas used is argon in this case. It is a noble gas so it does not interact chemically with either the substrate or the powder. It is used also as an insulator so neither the laser or the powder interacts with the air causing impurities or any other undesired results.

In the Table 2.1.2 the parameters used for this test are presented.

Variable	Value
Speed [mm/s]	7
Powder mass flow [units/rotation]	0.9
Pressure feeder [l/min]	5
Argon Pressure [l/min]	15

Table 2.1.2: Parameters used in this test

There were three test samples produced in this test, with different spot sizes each: 0.12 μm, 0.2 μm, 0.3 μm.

Once this test is conducted, the width of the tracks will be measured using the microscope. After that, the samples will be cut, mounted and polished for measure the height of the clads, and further crystallographic investigation.

Overlapping Test

With the data from the previous test, the width parameters are introduced into the machine and an overlapping test is performed. This test consist of

making deposition with different levels of overlapping, in this case there will be single tracks, 0%, 30% and 45%.

The aim of this test is to measure the height of the clads for each value of overlapping, in order to be able to perform a consistent coating later consisting of multiple layers. The layer height, as mentioned previously, is an input parameter on the machine, so it is necessary to obtain it experimentally. The power levels studied for this test will be 30% and 35%, with a spot size of 0.3 μm.

2.2 Sample Preparation

2.2.1 Cutting and Grinding

The cutting of the samples was performed by the *Delta AbrasiveMet Abrasive Cutter*, from Buehler. This machine consist of a spinning disc 102511N at 3600 rev/min, made of Al_2O_3, with a wheel size of 235x1.5x32mm, made specially to cut soft to medium hard steels[9].

The part is fixed into the base with one or two grips, depending on its geometry (Figure 2.2.1). Then, manually and slowly the blade is moved to get in contact with the test sample and being able to cut it.

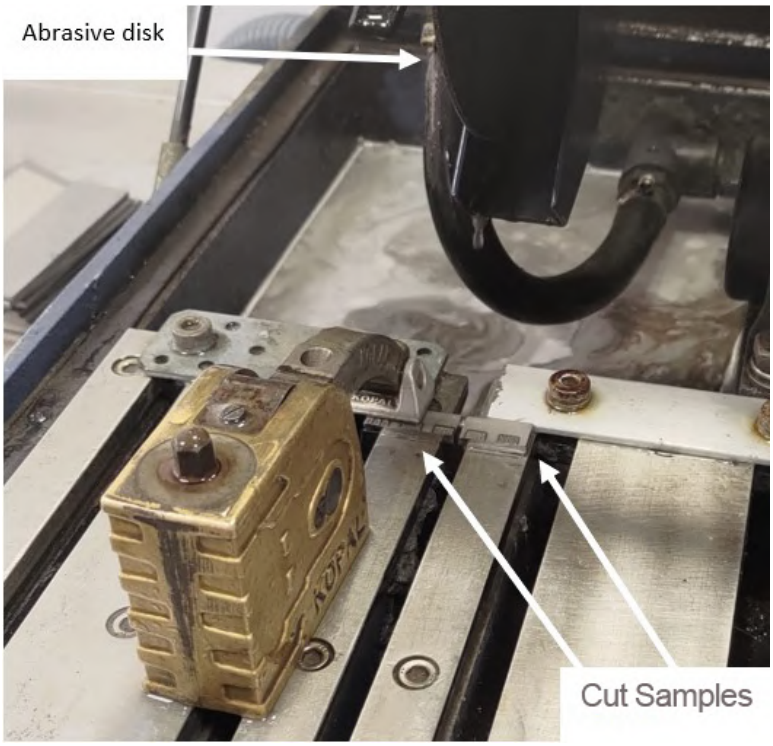

Figure 2.2.1: Cut samples

It is important to perform the cut slowly, otherwise the blade can be broken.

This can also happen if the material that is being cut is too hard for the blade.

The blade is cooled in the whole process with water to extend its lifetime and its working time.

This process is necessary because the maximum size of the samples in order to fit inside the hot mounting machine is 30mm.

2.2.2 Mounting

Mounting is the process of putting the samples into resin. This step is necessary to ensure a good flat position of the of the surface of interest for the polishing process, as well as the microscope examination later on.

Hot Mounting

Once the samples are cut in an appropriate size, its time to mount them. For this *SimplyMet 1000*, from Buehler was used (Figure 2.2.2). This is a hot mounting machine because it uses heat and pressure to obtain the mounted samples.

The procedure was to take the cut part and place the face of interest down on the surface of the machine. Then, the surface is lowered and the *MultiFast* phenolic resin powder[10] is added. The mounting parameters can be found on Table 2.2.1. After the hot mounting process is completed, a mounted sample ready for polishing is produced, Figure 2.2.3.

Figure 2.2.3: Hot mounted sample

Figure 2.2.2: Mounting machine

Variable	Value
Pressure [bar]	290
Heat time [min]	2
Cooling time [min]	4
Temperature of the process [ºC]	150

Table 2.2.1: Hot mounting parameters.

Cold Mounting

The cold mounting process has the advantage that there is no limit in regard of the size of the sample, but it is a much more tricky and less standardised process.

The goal is the same as the hot mounting, put the test sample into resin to ensure a flat surface to look at in the microscope. The sample is put into resin trying to ensure a vertical position, so it can be as flat as possible.

Tinfoil is used as a mold, trying to achieve a regular shape. When the resin is cured the tinfoil is removed and the mounted sample is obtained.

As it is a manual process, there is the potential for errors in the positioning of the sample, so in the later grinding and polishing process, the sample can be

worked to try to achieve a flatter surface.

2.2.3 Polishing

With the samples mounted its time to polish. The polishing process is necessary to ensure a good flat surface of the metal so the microscope can focus correctly. For this, *Beta Grinder-Polisher* from Buehler was used (Figure 2.2.4).

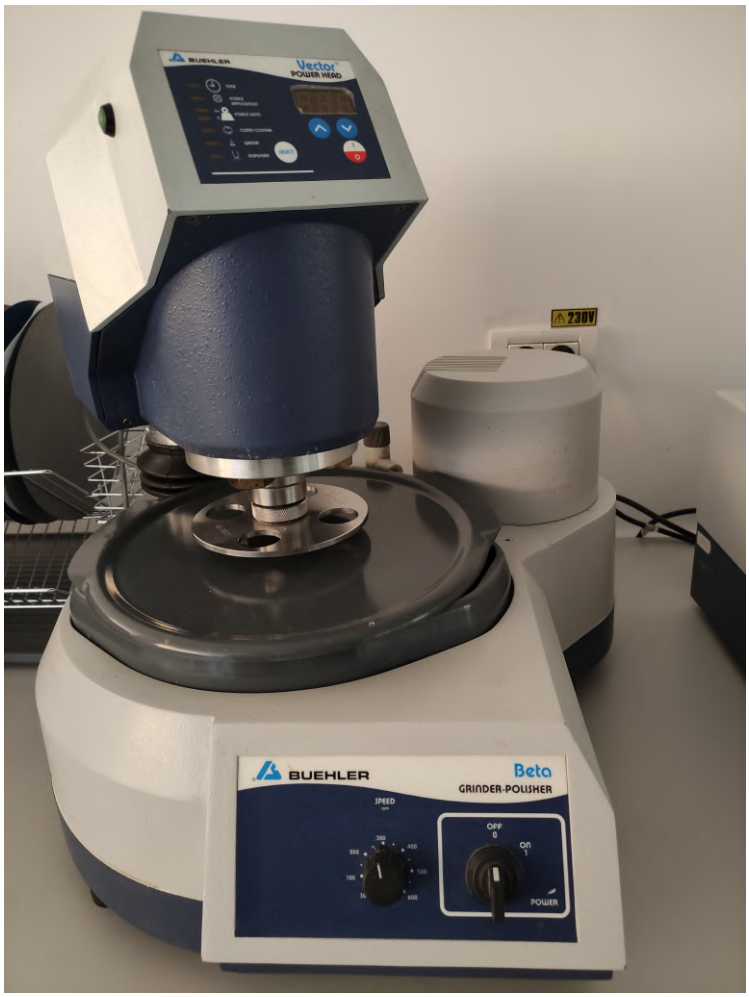

Figure 2.2.4: Grinding and polishing machine

The process followed was an standardised one provided by the manufacturer for this kind of steel, the details can be consulted on Table 2.2.2.

Stage	Surface	Abrasive	Lubricant	Time [min]	Force [N]	Speed [U/min]	Rotation
Planar Grinding	SiC-Paper	P320	Water	Until Plan	30	300	Comp
Sample Integrity	TexMet P	MetaDi Supreme 9 μm	MetaDi Fluid	3-5	30	150	Comp
	VerduTex	MetaDi Supreme 3 μm	MetaDi Fluid	3	30	150	Comp
Final Polishing	ChemoMet	MasterPrep 0.05 μm	dest Wasser	1-2	25	150	Comp

Table 2.2.2: Polishing parameters.

2.2.4 Etching

The last step prior to examining the test sample under the microscope is to etch it. The goal of etching the sample is to reveal the phases of steel, to be able to distinguish them visually.

The etchants are usually diluted acids like Nital, which is a combination of nitric acid and ethanol, or Picral, which is picric acid and ethanol. The effect on the microstructure of the steel is different, the etchant is chosen depending on which features of the microstructure is more relevant to analyze.

The acid chosen for this case was Nital. The etching procedure is based on trial and error. Too much etching leads to a burned sample, while too little results in no effect.

As it was mentioned previously, the surface of the sample has to be perfectly flat in this step.

Once the etching is performed, the microstructure can be studied making use of the optic microscope.

2.3 Microhardness

Microhardness tests will be conducted using the machine showed in Figure 2.3.1. This is an optical microscope as well as a microhardness machine.

The software of this machine is capable of performing microhardness tests following the standard [11] in an automatic way once the test points has been selected. This was crucial to save time and automatize the task, since as it will

be shown in the 4 section, many measurements were performed to check if the power level of the laser has any impact on this magnitude.

The test methodology was to perform 4 indentations in each track of the test sample obtained with the power levels showed in Table 2.1.1. The aim of this is to check if there is any correlation between hardness and power level of the laser.

Figure 2.3.1: Microhardness and microscope

2.4 Microstructure

Once the features are revealed after the etching phase, it will be possible to analyze the features of the microstructure of the test sample.

The microstructure of the clad will be analyzed to check the shape and the size of the grains, which will affect the properties. The dilution zone will also be measured. It is interesting to measure this zone because its width is directly related with the cooling rate, as well as the heat affected zone.

The microstructure and the dilution zone will be studied in a test sample with spot size 0.3mm, power level 40%, and different overlappings.

CHAPTER 3

Results

3.1 Power and spot size test

In this section are the results of the experiments explained in the section above.

3.1.1 Determination of the track width

The goal of this test was to gather data of the width of the tracks for a combination of laser power and spot size parameters, as previously commented in the prior section. In the Table 3.1.1, Table 3.1.2, Table 3.1.3 there is a sum up of the experimental results, which can be checked in the full extent in the section 5.1. Also, the test samples can be consulted in section 5.2.

Power Level [%]	Power Level [W]	Width [mm]
10	60	0.1372
15	90	0.17356
20	120	0.2978
25	150	0.3763
30	180	0.443
35	210	0.52326
40	240	0.57889
45	270	0.6634
50	300	0.6793
55	330	0.758778
60	360	0.79122
65	390	0.83311
70	420	0.886778
75	450	0.89178

Table 3.1.1: Table showing the power width of the tracks for each power level, for 0.12mm spot size.

Power Level [%]	Power Level [W]	Width [mm]
10	60	0.14811
15	90	0.179
20	120	0.22311
25	150	0.26288
30	180	0.52477
35	210	0.74944
40	240	0.86644
45	270	0.996
50	300	1.0844
55	330	1.23133
60	360	1.3407
65	390	1.362
70	420	1.4691
75	450	1.56089

Table 3.1.2: Table showing the power width of the tracks for each power level, for 0.2mm spot size.

Power Level [%]	Power Level [W]	Width [mm]
10	60	-
15	90	-
20	120	0.23433
25	150	0.4121
30	180	0.571
35	210	0.74622
40	240	0.8321
45	270	0.94344
50	300	1.02789
55	330	1.07978
60	360	1.1324
65	390	1.2584
70	420	1.27
75	450	1.44789

Table 3.1.3: Table showing the power width of the tracks for each power level, for 0.3mm spot size.

In the graph presented in the Figure 3.1.1 there is a direct comparison of the width of the track for each laser power for the three spot sizes. The data on this chart starts to be relevant from 30%, because smaller values do not melt the powder in many cases, so the results are nor really valid. The pictures of all the tracks can be consulted in **??**.

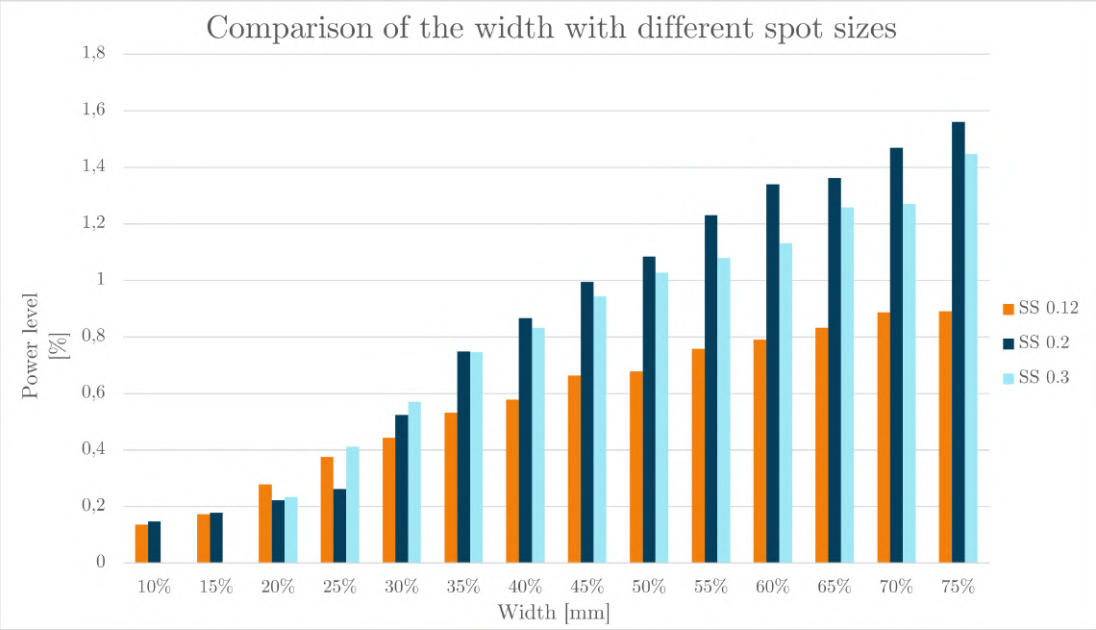

Figure 3.1.1: Bar chart with the comparison of the track width for different spot sizes and power levels.

The results shown in the Figure 3.1.1 are very interesting, because in a way they are counter intuitive. They show a trend in which the wider track does not correspond either to the biggest or the smallest spot size. The power is constant in each power level, which means that the wider the spot size, the less energy density is being applied. This helps to explain why the 0.3 mm spot size is consistently lower than the 0.2 mm.

However, with that reasoning it would be logical that the 0.12 mm spot size would provide the widest track, and as it can be seen this is not the case. This is due to the relationship between the powder size and the spot size. The powder used in this test is the *MetcoAdd 316L-D*, with a particle size of 106+15 μm. This means that no more than one particle of the powder can be at the same time under the laser, which limits its ability to form a coat.

3.2 Track height

Regarding the track height, in Figure 3.2.1 it can be seen the results of the measurements. The raw measurements can be consulted in section 5.3. The measurements were performed on one test sample per power level and overlapping value.

As it can be seen on the chart, it looks like there is a trend correlating the increasing of the overlapping and the increasing of the track height. It also seems like increasing the power level also increases the track height.

However this results must be taken with a grain of salt, because there are cases in which they does not apply, such as in the 45% power level. It is also worth noting that track height value for the 30% power level and the 15% overlapping is missing, this was due to an error in the power feeder of the laser cladding machine, which turned the results of this test sample invalid.

As mentioned above, the results of the track height appear to follow a trend, however there is not enough data to confirm it in a proper way. More data from several identical test samples would be needed to actually confirm it.

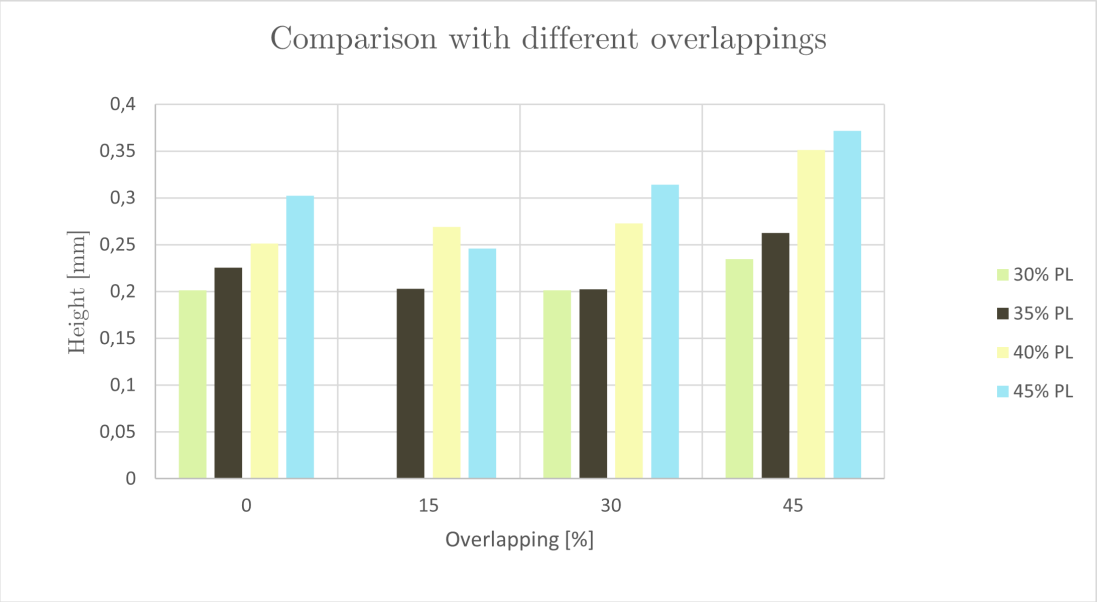

Figure 3.2.1: Bar chart showing the results of the measurements of the track height for different overlappings and power levels.

3.3 Microstructure

Regarding the microstructure analysis of the clad, in Figure 3.3.1 there is a micrography of a clad, in which it can be seen the variation of the grain shape of it. Near the surface the grain have more equiaxial shape, while closer to the base material they tend to have more of a columnar shape.

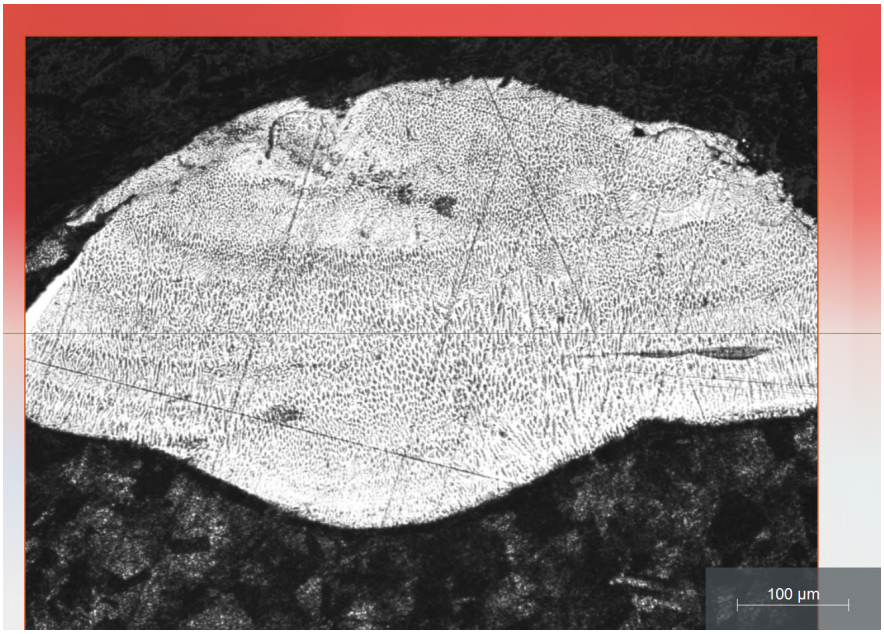

Figure 3.3.1: Micrography of the clad. Spot size 0.3mm, Power Level 40%, Overlapping 30%

This has to do with the cooling gradient. With higher cooling gradients, the grains grow in the direction of the heat flow. The grains grow in a columnar shape next to the clad material, as the heat can escape faster through the metal due to it higher thermal conductivity compared with calm air in the other side. In figures 3.3.2a and 3.3.2b it is presented a closer look at the shape of the grains. It can be also observed that the grain sizes of the clad material are significantly smaller than the ones in the base material. This is due to the rapid cooling of the clad.

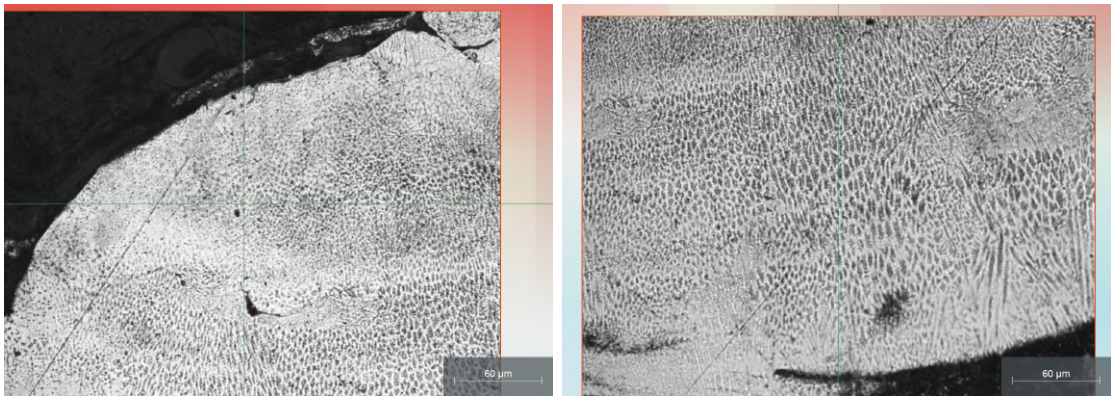

(a) (b)

Figure 3.3.2: Micrography of the different regions of the clad. (a) Shows the exterior part, while (b) shows the inner. Spot size 0.3mm, Power Level 40%, Overlapping 30%

3.4 Dilution Zone

The dilution zone is the area in which the clad and base material are fused.

In the Figure 3.4.1 it can be seen the zone, with the measurement. As it is shown, the dimensions of this zone is several orders of magnitude smaller than the height of the clad (Figure 3.2.1).

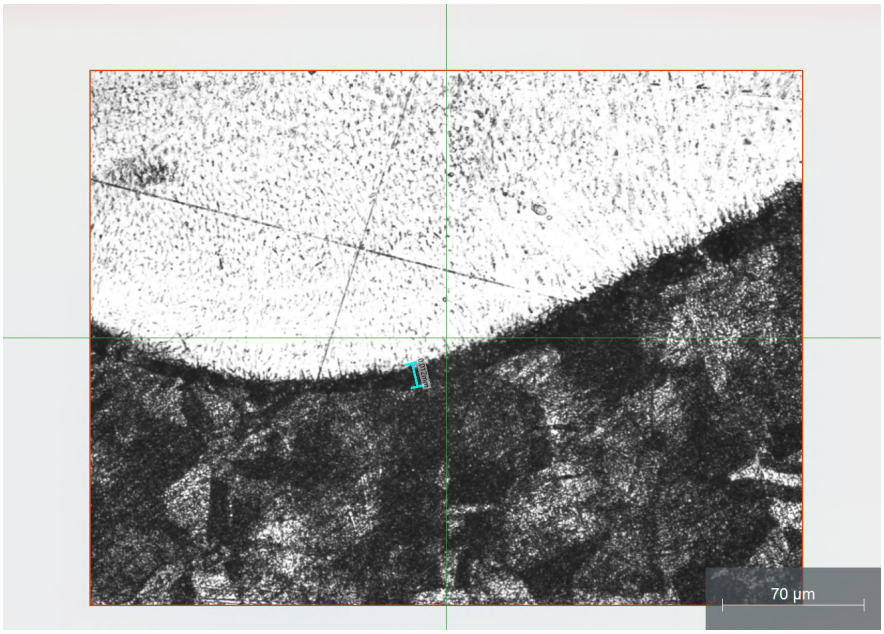

Figure 3.4.1: Micrography of the dilution zone. Spot size 0.3mm, Power Level 40%, Overlapping 30%

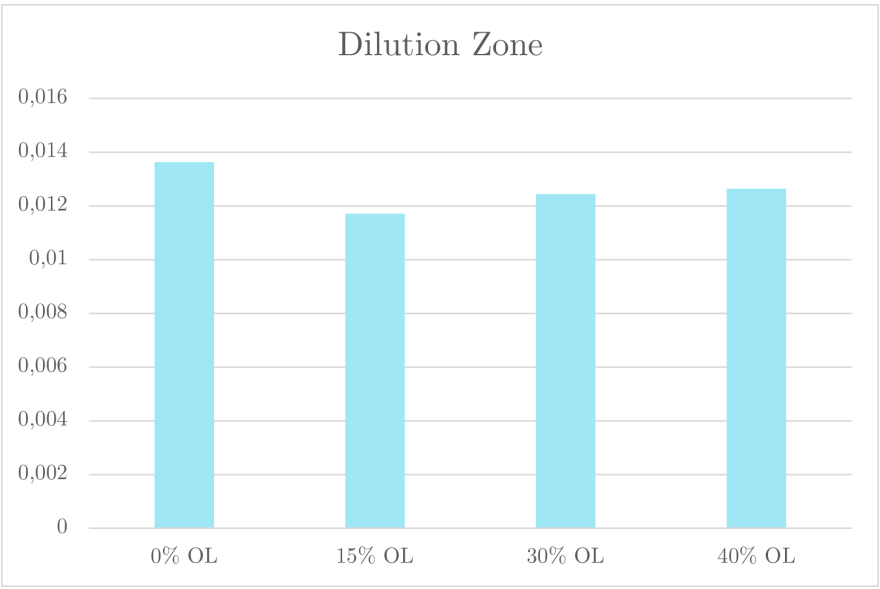

Figure 3.4.2: Chart showing a sum up of the measurements in the dilution zone for 40% power level, for different levels of overlapping.

The chart shown in Figure 3.4.2 shows a comprehensive summary of all the measurements taken in the test sample. The test sample was produced using 40% power level, with different levels of overlapping. As it can be seen there is no direct correlation between overlapping and size of the dilution zone, as they are all very small.

It would be interesting to check for correlations between power level and size of the dilution zone. Due to lack of test samples this study was not able to be made.

3.5 Microhardness

About the microhardness and its relationship with the power level there is not much correlation to be seen, as it is shown in Figure 3.5.1.

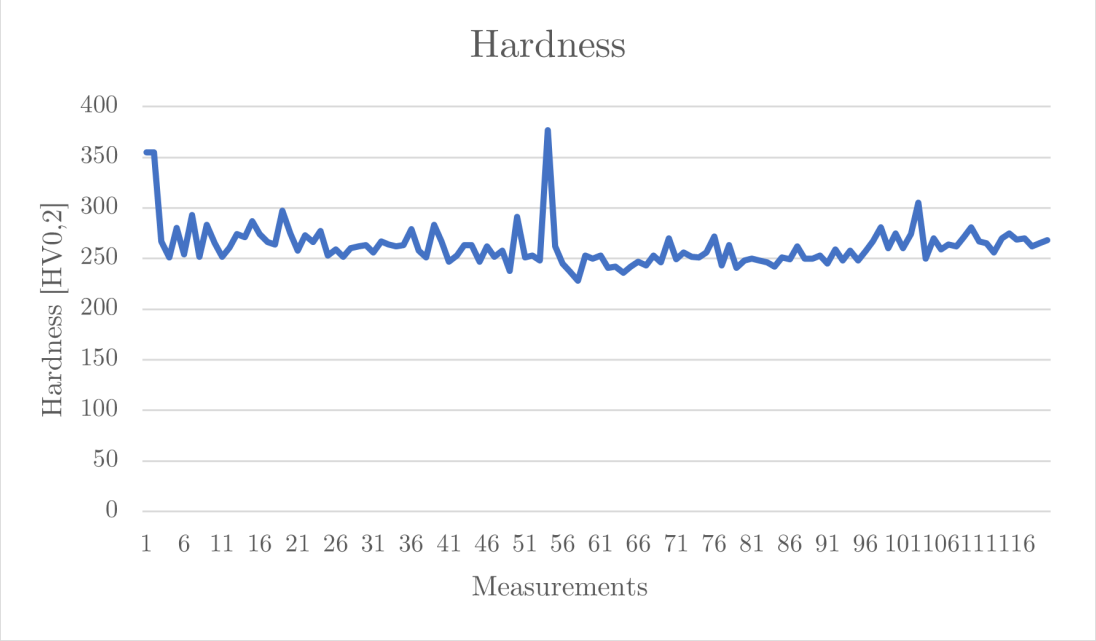

Figure 3.5.1: Graph showing the measurements of HV0.2 microhardness test performed on the 0.3mm spot size test sample for several power levels.

In this graph are represented all the measurements taken. The measurements are arranged in a way that the first ones are at 75% power level, and the last ones at 30%. As it was mentioned above, there were 4 measurements taken in each power level. At first sight it can appear that the results obtained are erratic, however upon further inspection of the indents (available in the appendix 5.5). It can be seen that the measurements that vary the most are mostly the first ones, this is because the grinding methods used in this test samples was manual, as they were cold mounted, so it produces less consistent results.

It can be seen that, as the surface smooths, so does the variation of values.

This indicates no direct correlation between power level and hardness of the clad.

CHAPTER 4

Conclusions and Future Work

In this section a summary of all the conclusions reached in this study will be made, as well as propose starting points for future studies.

First, the width of the track is correlated with the spot size and the power level. The higher the power level, the wider the track. Regarding the spot size there is the need to take into account the energy density, as well as the relationship between the spot size and the particle size of the powder used.

Regarding the track height there was a slight correlation found between increasing the overlapping and the power level and its value. However this has to be tested further because of the lack of test samples to confirm the results. The confirmation of this trend with a proper number of test samples would be a good starting point for future work.

With respect to the microstructure, the difference in size in the grains of the clad and the base material is clear. It is also worth mentioning the difference in shape of the grains in the clad closer to the outside and closer to the base metal.

Related to this is the dilution zone. There was no correlation found between the overlapping and the width of the dilution zone. For future studies would be interesting to check the correlation of this value with other parameters such as power level.

The microhardness analysis shows no correlation between the power level and the hardness of the clad. This is interesting, as it seems to be an independent parameter. An idea for future work could be studying the parameters that actually affects the microhardness of the clad.

CHAPTER 5

Appendix

5.1 Table containing the width of the tracks with different power levels

This chart contains all the experimental data gathered in the experiment regarding the track width. There were three tracks per power level, and three measurements were taken in each of them. For the final result all of this measurements were averaged. The bars represent the deviation between groups of measurements, the more uneven the bars the more deviation in that regard. It can be seen that, as the power level rises, this deviation gets smaller.

Power [W]	Power level [%]	Track	316LSI-Ls0,12 [mm]			316LSI-Ls0,2 [mm]			316LSI-Ls0,3 [mm]		
			Width Measurements [mm]	Mean (Track) [mm]	Mean [mm]	Width Measurements [mm]	Mean (Track) [mm]	Mean [mm]	Width Measurements [mm]	Mean (Track) [mm]	Mean [mm]
60	10%	1	0,167 0,186 0,180	0,178	0,137	0,148 0,154 0,150	0,151	0,148		0,000	0,000
		2	0,131 0,126 0,124	0,127		0,157 0,143 0,148	0,149			0,000	
		3	0,107 0,107 0,107	0,107		0,132 0,145 0,156	0,144			0,000	
90	15%	1	0,175 0,180 0,177	0,177	0,174	0,178 0,186 0,184	0,183	0,179		0,000	0,000
		2	0,192 0,179 0,165	0,179		0,171 0,184 0,178	0,178			0,000	
		3	0,166 0,162 0,166	0,165		0,176 0,177 0,177	0,177			0,000	
120	20%	1	0,275 0,286 0,268	0,276	0,280	0,230 0,231 0,230	0,230	0,223	0,159 0,158 0,165	0,161	0,234
		2	0,293 0,273 0,283	0,283		0,219 0,228 0,228	0,225		0,185 0,157 0,168	0,170	
		3	0,286 0,283 0,271	0,280		0,215 0,210 0,218	0,214		0,355 0,370 0,392	0,372	
150	25%	1	0,389 0,379 0,376	0,381	0,376	0,259 0,263 0,265	0,262	0,263	0,442 0,413 0,403	0,419	0,412
		2	0,370 0,366 0,365	0,367		0,256 0,250 0,250	0,252		0,356 0,414 0,429	0,400	
		3	0,384 0,379 0,379	0,381		0,296 0,269 0,258	0,274		0,421 0,400 0,431	0,417	
180	30%	1	0,443 0,450 0,444	0,446	0,443	0,523 0,528 0,525	0,525	0,525	0,587 0,585 0,591	0,588	0,571
		2	0,444 0,446 0,432	0,441		0,523 0,522 0,527	0,524		0,559 0,569 0,567	0,565	
		3	0,446 0,443 0,439	0,443		0,497 0,548 0,530	0,525		0,578 0,544 0,559	0,560	
210	35%	1	0,530 0,529 0,525	0,528	0,533	0,750 0,734 0,735	0,740	0,749	0,740 0,733 0,778	0,750	0,746
		2	0,548 0,540 0,531	0,540		0,745 0,743 0,773	0,754		0,760 0,715 0,705	0,727	
		3	0,536 0,531 0,524	0,530		0,773 0,753 0,739	0,755		0,769 0,772 0,744	0,762	
240	40%	1	0,581 0,578 0,572	0,577	0,579	0,862 0,885 0,860	0,869	0,866	0,816 0,868 0,846	0,843	0,832
		2	0,572 0,578 0,575	0,575		0,889 0,861 0,865	0,872		0,817 0,828 0,860	0,835	
		3	0,584 0,581 0,589	0,585		0,861 0,863 0,852	0,859		0,775 0,838 0,841	0,818	

270	45%	1	0,663 0,658 0,668	0,663	0,663	1,003 0,972 0,980	0,985	0,996	0,943 0,924 0,921	0,929	0,943
		2	0,681 0,660 0,665	0,669		0,990 1,020 1,014	1,008		0,941 0,954 0,961	0,952	
		3	0,665 0,650 0,661	0,659		0,982 0,997 1,006	0,995		0,941 0,960 0,946	0,949	
300	50%	1	0,662 0,671 0,682	0,672	0,679	1,061 1,073 1,070	1,068	1,084	0,950 1,022 1,078	1,017	1,028
		2	0,677 0,695 0,680	0,684		1,102 1,103 1,110	1,105		0,992 1,048 1,076	1,039	
		3	0,699 0,682 0,666	0,682		1,099 1,056 1,086	1,080		0,945 1,054 1,086	1,028	
330	55%	1	0,759 0,757 0,749	0,755	0,759	1,208 1,233 1,221	1,221	1,231	1,077 1,086 1,079	1,081	1,080
		2	0,790 0,759 0,724	0,758		1,222 1,228 1,243	1,231		1,089 1,076 1,085	1,083	
		3	0,762 0,767 0,762	0,764		1,228 1,255 1,244	1,242		1,072 1,079 1,075	1,075	
360	60%	1	0,792 0,781 0,763	0,779	0,791	1,357 1,335 1,323	1,338	1,341	1,134 1,168 0,949	1,084	1,132
		2	0,812 0,793 0,789	0,798		1,351 1,367 1,350	1,356		1,131 1,160 1,184	1,158	
		3	0,801 0,807 0,783	0,797		1,343 1,302 1,338	1,328		1,133 1,164 1,169	1,155	
390	65%	1	0,827 0,818 0,829	0,825	0,833	1,350 1,348 1,380	1,359	1,362	1,233 1,239 1,267	1,246	1,258
		2	0,847 0,842 0,842	0,844		1,361 1,338 1,393	1,364		1,240 1,247 1,275	1,254	
		3	0,842 0,824 0,827	0,831		1,349 1,396 1,343	1,363		1,268 1,292 1,265	1,275	
420	70%	1	0,868 0,873 0,887	0,876	0,887	1,474 1,424 1,476	1,458	1,469	1,240 1,270 1,290	1,267	1,270
		2	0,892 0,883 0,897	0,891		1,452 1,476 1,504	1,477		1,218 1,260 1,286	1,255	
		3	0,882 0,907 0,892	0,894		1,482 1,482 1,452	1,472		1,276 1,278 1,312	1,289	
450	75%	1	0,879 0,884 0,886	0,883	0,892	1,550 1,598 1,565	1,571	1,561	1,399 1,422 1,477	1,433	1,448
		2	0,888 0,893 0,897	0,893		1,591 1,585 1,526	1,567		1,410 1,430 1,449	1,430	
		3	0,879 0,918 0,902	0,900		1,527 1,531 1,575	1,544		1,437 1,503 1,504	1,481	

5.2 Track width samples

5.2.1 0.12mm spot size

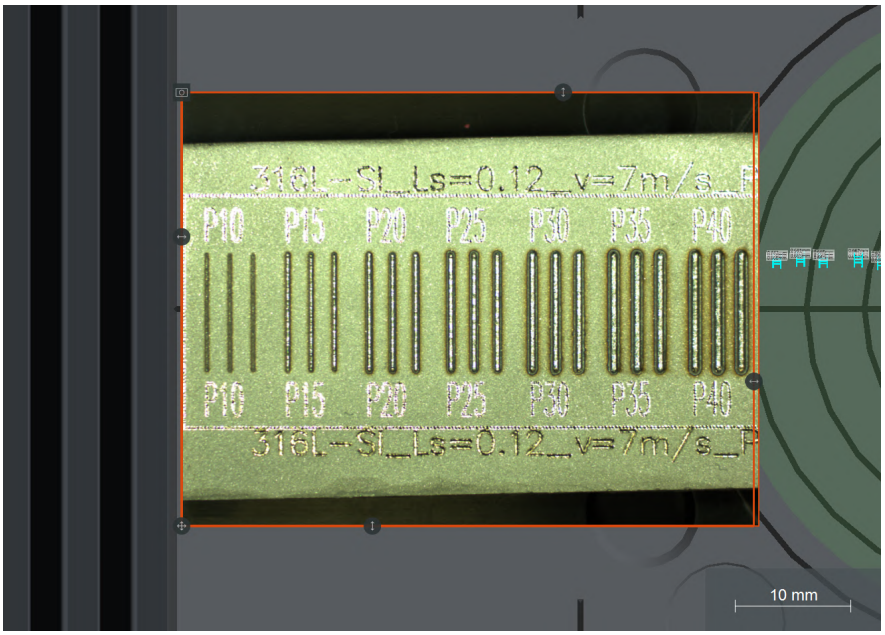

Figure 5.2.1: Overview image from the microscope of the 0.12 mm spot size sample, for 10% to 40% power level.

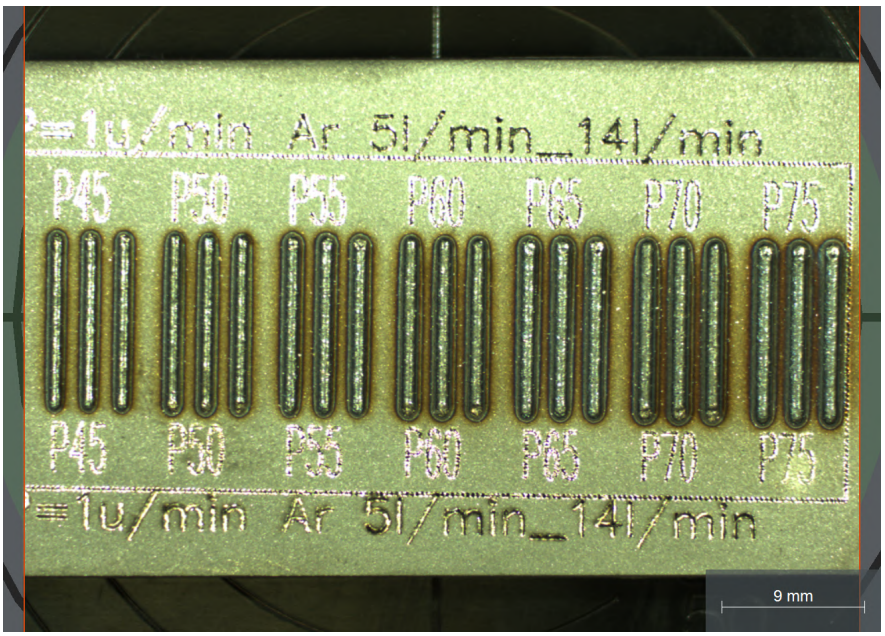

Figure 5.2.2: Overview image from the microscope of the 0.12 mm spot size sample, for 40% to 75% power level.

5.2.2 0.2mm spot size

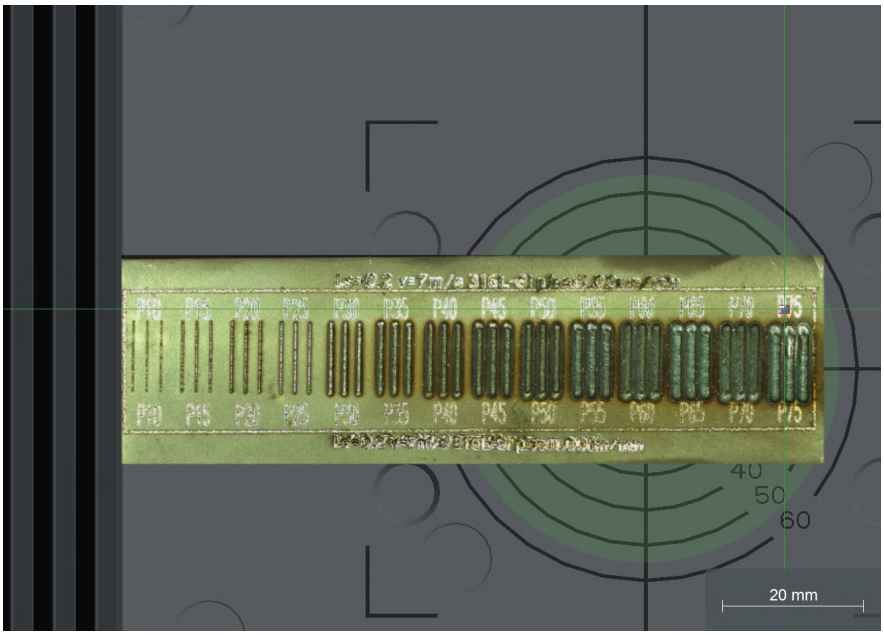

Figure 5.2.3: Overview image from the microscope of the 0.2 mm spot size sample.

5.2.3 0.3mm spot size

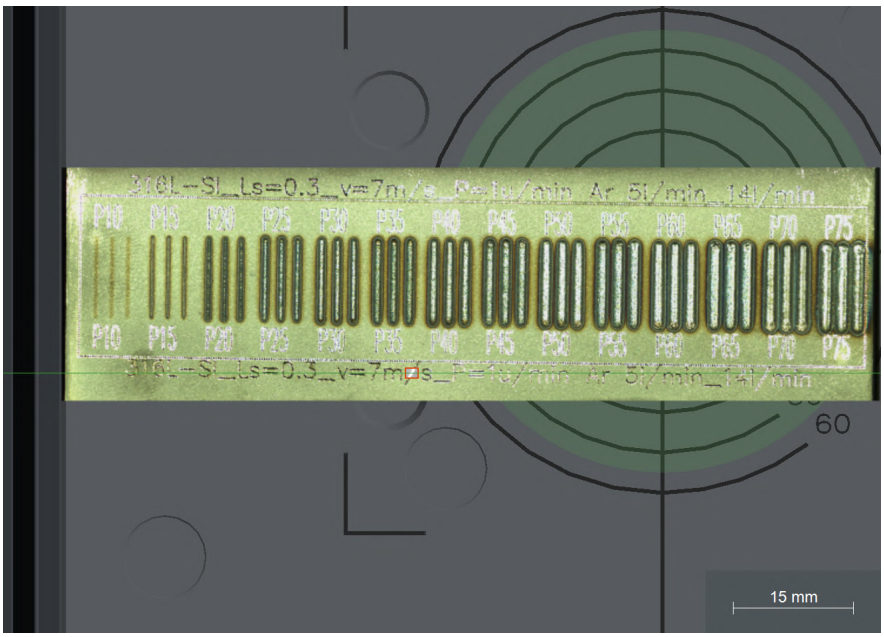

Figure 5.2.4: Overview image from the microscope of the 0.3 mm spot size sample.

5.3 Track height samples

5.3.1 Power Level 35

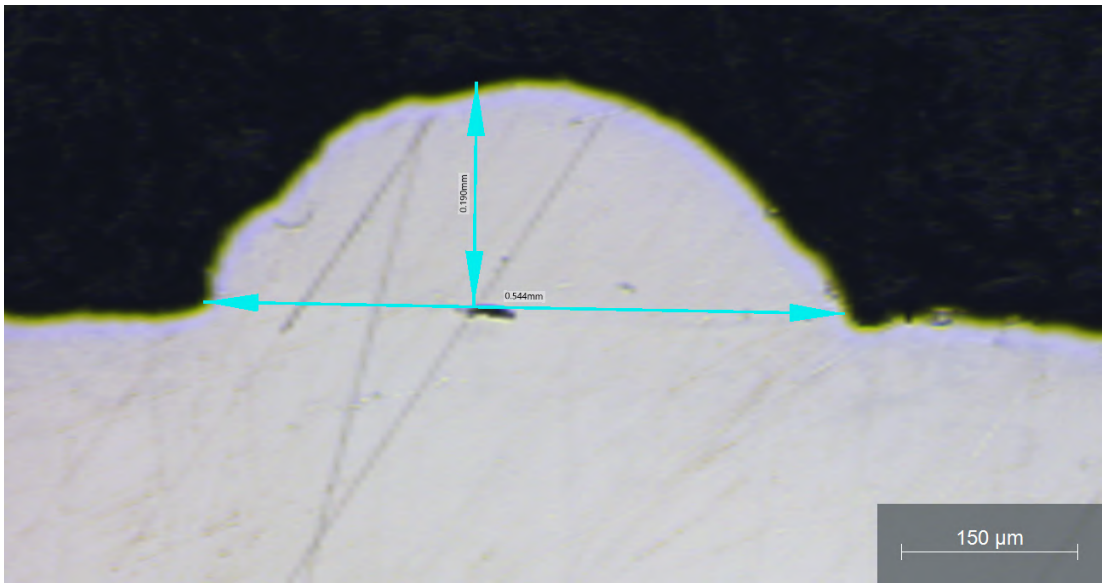

Figure 5.3.1: Measurements on a single track for 30 power level (1).

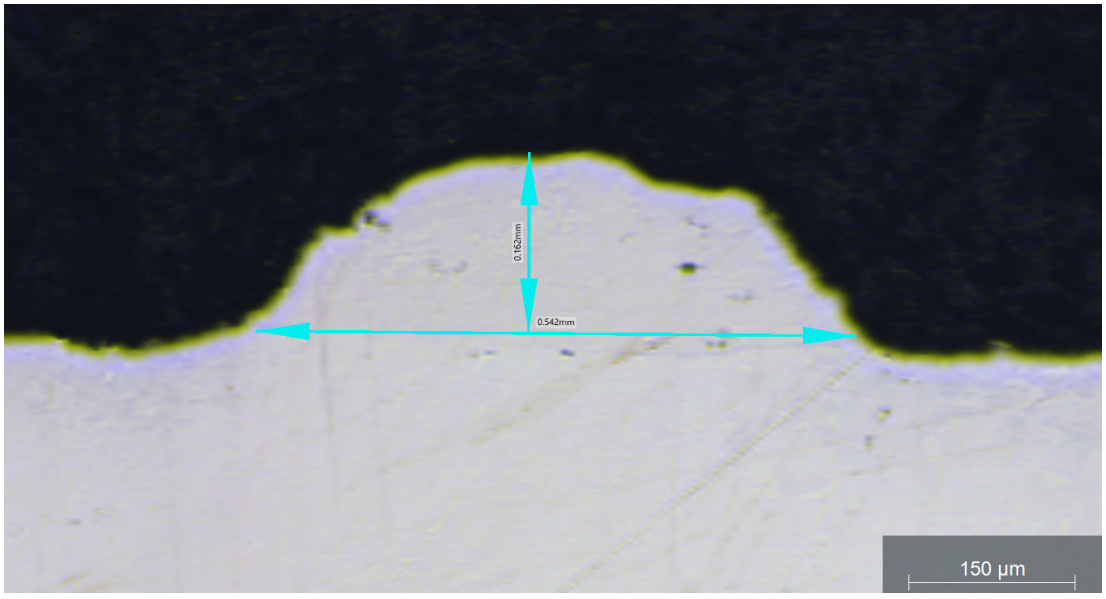

Figure 5.3.2: Measurements on a single track for 30 power level (2).

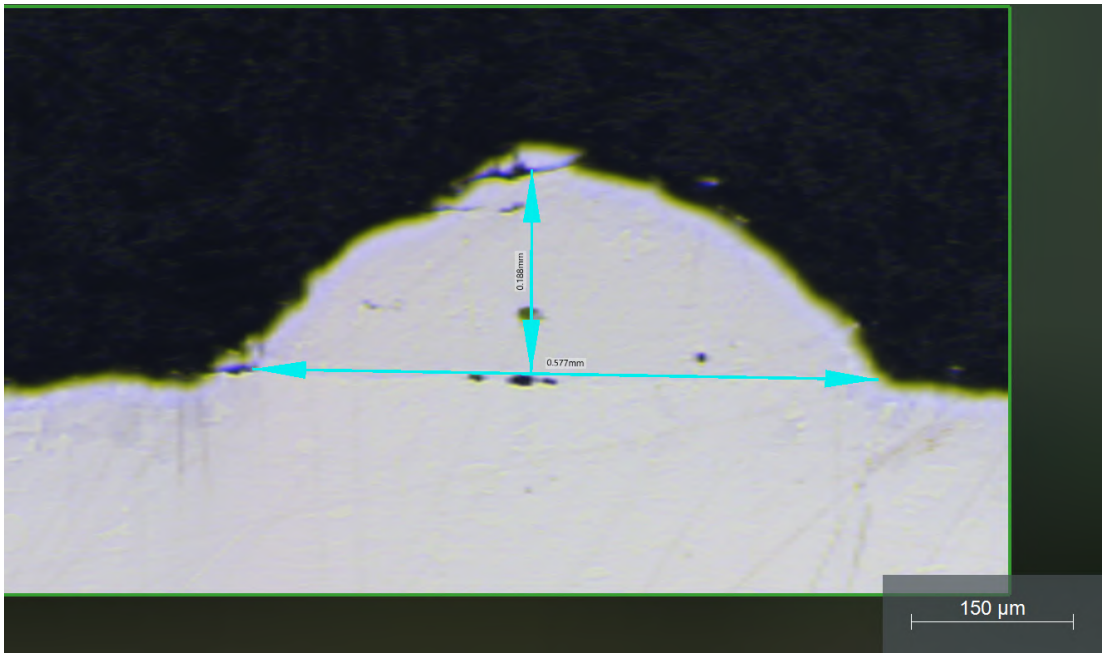

Figure 5.3.3: Measurements on a single track for 30 power level (3).

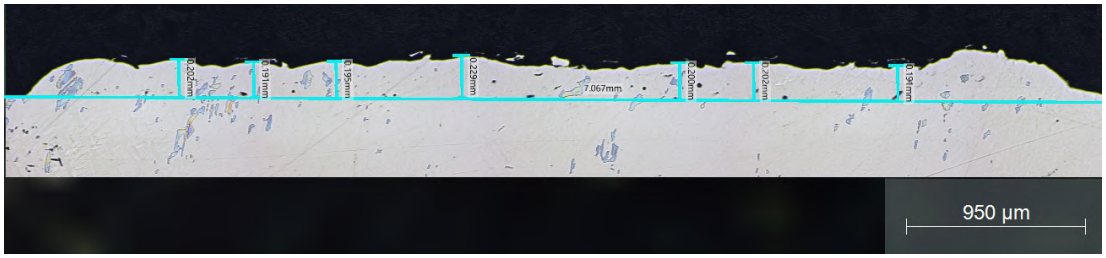

Figure 5.3.4: Measurements on 30% overlap for 30 power level.

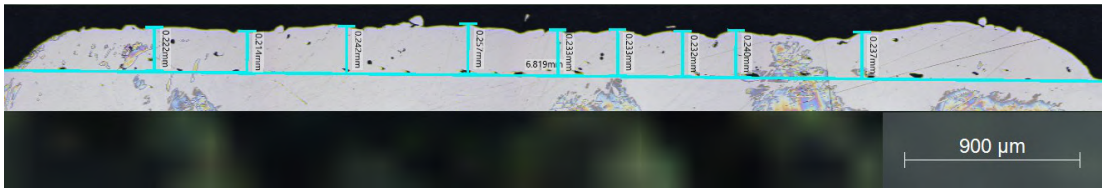

Figure 5.3.5: Measurements on 45% overlap for 30 power level.

5.3.2 Power Level 45

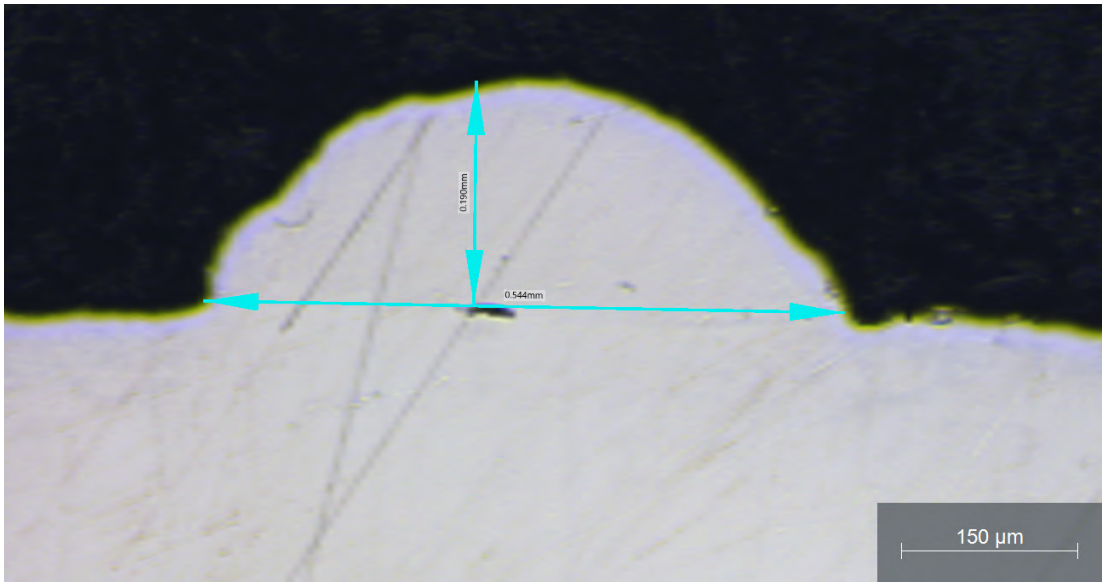

Figure 5.3.6: Measurements on single track for 35 power level (1).

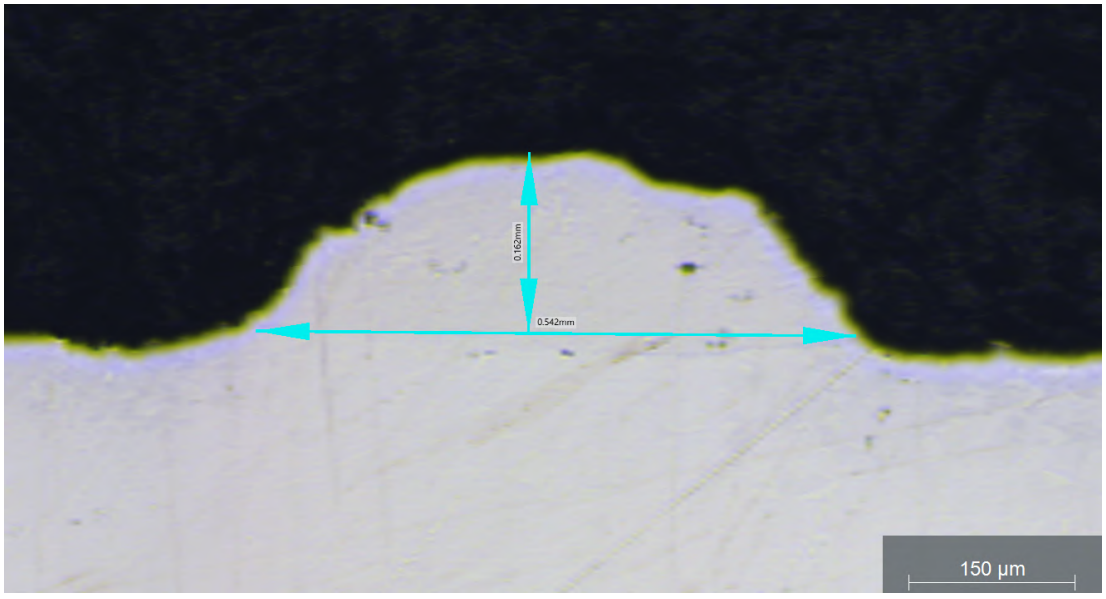

Figure 5.3.7: Measurements on single track for 35 power level (2).

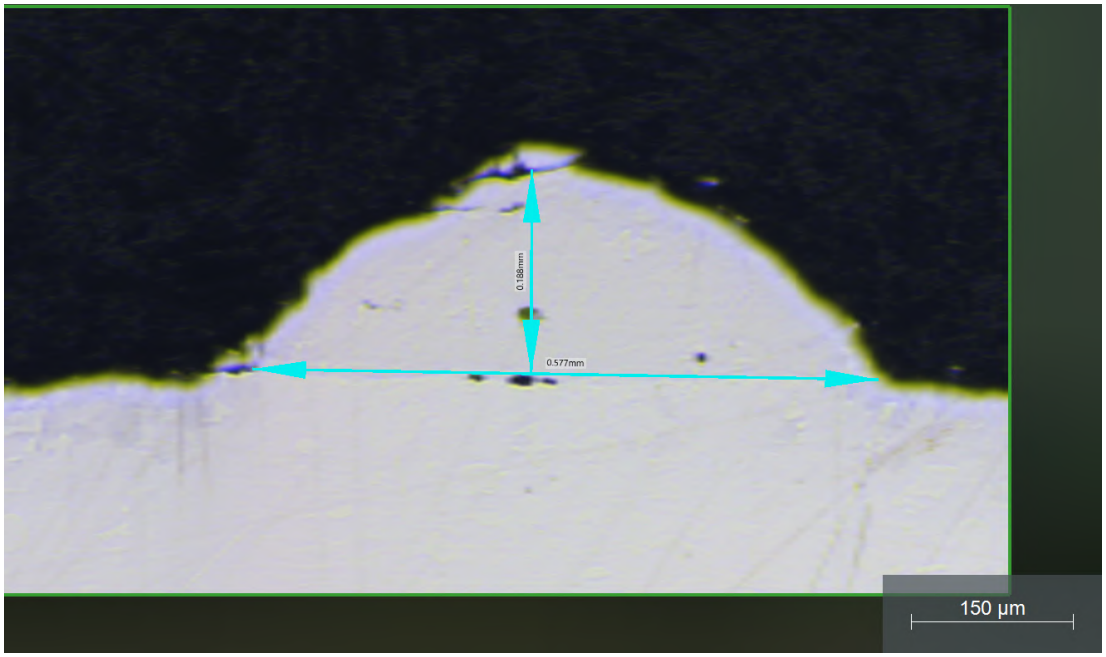

Figure 5.3.8: Measurements on single track for 35 power level (3).

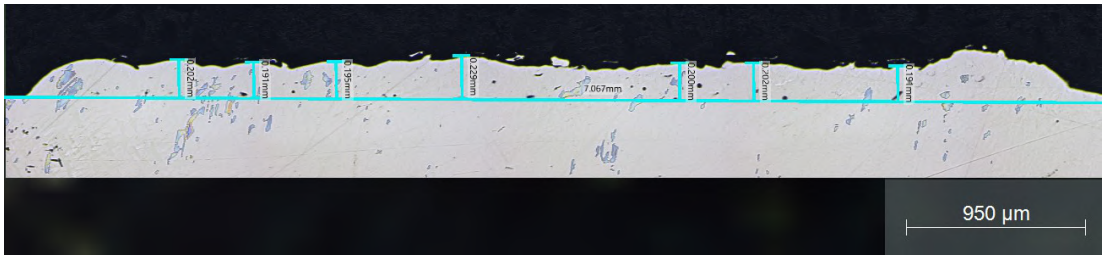

Figure 5.3.9: Measurements 30% overlapping for 35 power level.

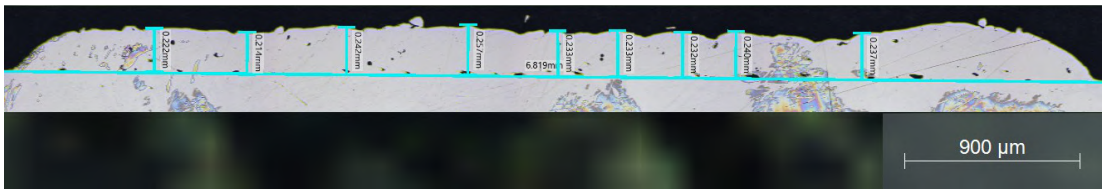

Figure 5.3.10: Measurements 45% overlapping for 35 power level.

5.4 Table containing the height of the tracks with different overlappings and power levels

This chart contains all the experimental data gathered in the experiment regarding the track height. There were three power levels studied, and 4 levels of overlapping per power level, apart from the single tracks. For the final result all of this measurements were averaged. The bars represent the deviation between groups of measurements, the more uneven the bars the more deviation in that regard.

30% Power Level			35% Power Level			40% Power Level			45% Power Level		
Overlapping [%]	Measures [mm]	Average [mm]	Overlapping [%]	Measures [mm]	Average [mm]	Overlapping [%]	Measures [mm]	Average [mm]	Overlapping [%]	Measures [mm]	Average [mm]
Single Tracks	0,19	0,180	Single Tracks	0,183	0,180	Single Tracks	0,267	0,279	Single Tracks	0,247	0,247
	0,162			0,176			0,271			0,261	
	0,188			0,181			0,298			0,234	
0	0,236	0,201	0	0,22	0,225	0	0,268	0,251	0	0,248	0,303
	0,215			0,245			0,299			0,387	
	0,209			0,239			0,234			0,308	
	0,195			0,258			0,263			0,32	
	0,216			0,211			0,258			0,303	
	0,173			0,238			0,258			0,279	
	0,166			0,226			0,227			0,273	
				0,166			0,203				
15	error feeder	0,000	15	0,168	0,203	15	0,228	0,269	15	0,25	0,246
				0,189			0,259			0,264	
				0,198			0,289			0,182	
				0,232			0,28			0,28	
				0,184			0,283			0,299	
				0,202			0,254			0,225	
				0,221			0,271			0,223	
				0,23			0,254			0,235	
							0,303			0,224	
										0,283	
30	0,202	0,201	30	0,2	0,202	30	0,275	0,273	30	0,326	0,314
	0,191			0,212			0,268			0,256	
	0,195			0,195			0,26			0,277	
	0,229			0,226			0,283			0,313	
	0,2			0,213			0,306			0,342	
	0,202			0,184			0,221			0,349	
	0,191			0,186			0,287			0,333	
							0,281			0,292	
										0,313	
										0,34	
45	0,222	0,235	45	0,282	0,263	45	0,338	0,351	45	0,386	0,372
	0,214			0,259			0,325			0,403	
	0,242			0,25			0,319			0,382	
	0,257			0,236			0,348			0,397	
	0,233			0,229			0,322			0,36	
	0,233			0,287			0,334			0,402	
	0,24			0,292			0,393			0,361	
	0,237			0,269			0,404			0,327	
				0,272			0,406			0,37	
				0,251			0,339			0,33	
							0,318				
							0,361				
							0,356				

5.5 Microhardness measurements

In here, the report of the QATM software regarding the measurements of the hardness is presented, it consists first of a table with the values of all the measurements, and after that the pictures of the actual indentations and the measurements of the diagonals to get the value of hardness. The measurements of the diagonals were made automatically by the software.

Testing report

Sample

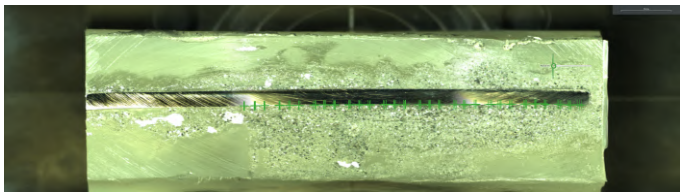

Test series

proba:

QWEQW:

WQRQWR:

No.	Hardness	Method	No.	Hardness	Method	No.	Hardness	Method
1	355	HV 0.2	2	355	HV 0.2	3	267	HV 0.2
4	251	HV 0.2	5	280	HV 0.2	6	254	HV 0.2
7	293	HV 0.2	8	252	HV 0.2	9	283	HV 0.2
10	265	HV 0.2	11	252	HV 0.2	12	261	HV 0.2
13	274	HV 0.2	14	271	HV 0.2	15	287	HV 0.2
16	274	HV 0.2	17	266	HV 0.2	18	264	HV 0.2
19	297	HV 0.2	20	275	HV 0.2	21	258	HV 0.2
22	273	HV 0.2	23	266	HV 0.2	24	277	HV 0.2
25	253	HV 0.2	26	259	HV 0.2	27	252	HV 0.2
28	260	HV 0.2	29	262	HV 0.2	30	263	HV 0.2
31	256	HV 0.2	32	267	HV 0.2	33	264	HV 0.2
34	262	HV 0.2	35	263	HV 0.2	36	279	HV 0.2
37	258	HV 0.2	38	251	HV 0.2	39	283	HV 0.2
40	267	HV 0.2	41	247	HV 0.2	42	253	HV 0.2
43	263	HV 0.2	44	263	HV 0.2	45	247	HV 0.2
46	262	HV 0.2	47	252	HV 0.2	48	258	HV 0.2
49	238	HV 0.2	50	291	HV 0.2	51	251	HV 0.2
52	253	HV 0.2	53	248	HV 0.2	54	377	HV 0.2
55	262	HV 0.2	56	245	HV 0.2	57	237	HV 0.2
58	228	HV 0.2	59	253	HV 0.2	60	250	HV 0.2
61	253	HV 0.2	62	241	HV 0.2	63	242	HV 0.2
64	236	HV 0.2	65	242	HV 0.2	66	247	HV 0.2
67	243	HV 0.2	68	253	HV 0.2	69	246	HV 0.2
70	270	HV 0.2	71	249	HV 0.2	72	256	HV 0.2
73	252	HV 0.2	74	251	HV 0.2	75	256	HV 0.2

Testing report

No.	Hardness	Method	No.	Hardness	Method	No.	Hardness	Method
76	272	HV 0.2	77	243	HV 0.2	78	263	HV 0.2
79	241	HV 0.2	80	248	HV 0.2	81	250	HV 0.2
82	248	HV 0.2	83	246	HV 0.2	84	242	HV 0.2
85	251	HV 0.2	86	249	HV 0.2	87	262	HV 0.2
88	250	HV 0.2	89	250	HV 0.2	90	253	HV 0.2
91	245	HV 0.2	92	259	HV 0.2	93	248	HV 0.2
94	258	HV 0.2	95	248	HV 0.2	96	257	HV 0.2
97	267	HV 0.2	98	281	HV 0.2	99	260	HV 0.2
100	275	HV 0.2	101	260	HV 0.2	102	274	HV 0.2
103	305	HV 0.2	104	250	HV 0.2	105	270	HV 0.2
106	259	HV 0.2	107	264	HV 0.2	108	262	HV 0.2
109	271	HV 0.2	110	281	HV 0.2	111	267	HV 0.2
112	265	HV 0.2	113	256	HV 0.2	114	270	HV 0.2
115	275	HV 0.2	116	269	HV 0.2	117	270	HV 0.2
118	262	HV 0.2	119	265	HV 0.2	120	268	HV 0.2

Statistics:

Mean value	Range	Hardness min.	Hardness max.	Standard dev.	Results OK
259.93	77	228	305	13.48	116

Test point images:

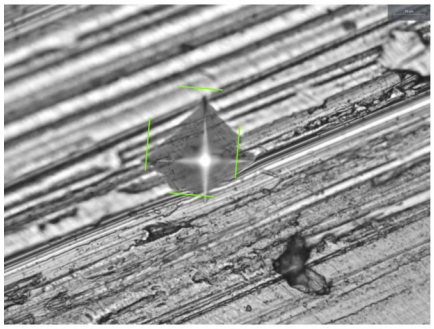

1 355 HV 0.2 0.03 0.04

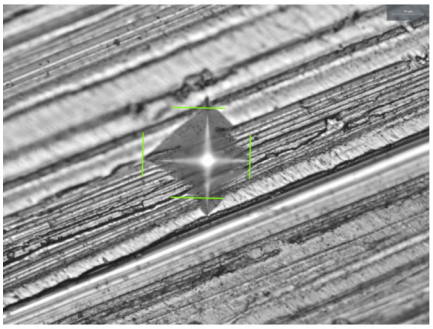

2 355 HV 0.2 0.04 0.03

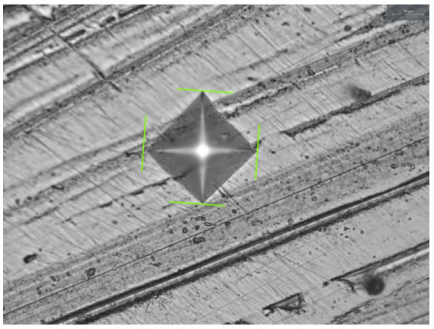

3 267 HV 0.2 0.04 0.04

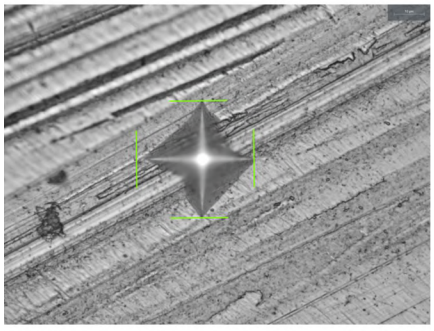

4 251 HV 0.2 0.04 0.04

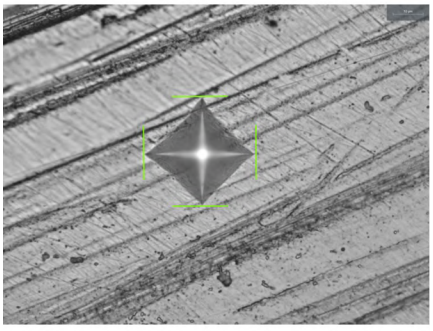

5 280 HV 0.2 0.04 0.04

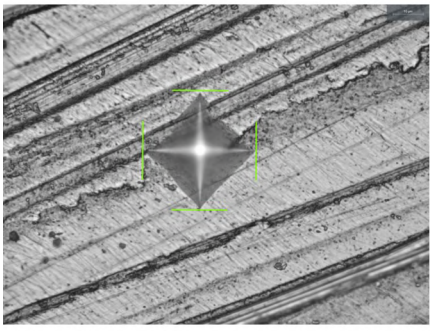

6 254 HV 0.2 0.04 0.04

Test point images:

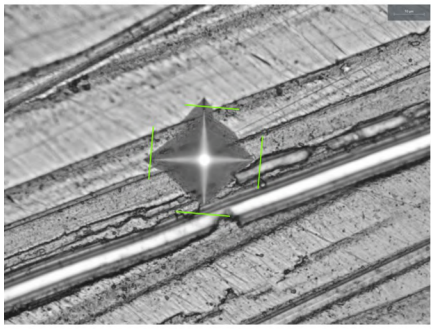

7 293 HV 0.2 0.04 0.04

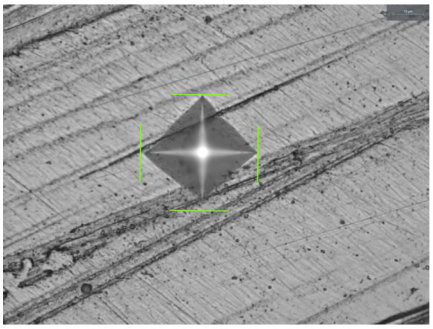

8 252 HV 0.2 0.04 0.04

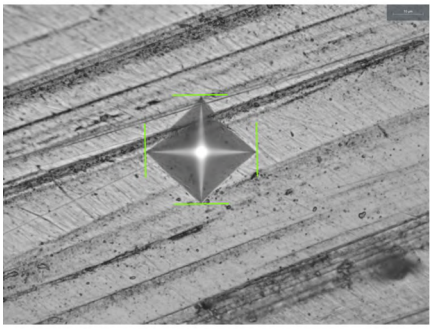

9 283 HV 0.2 0.04 0.04

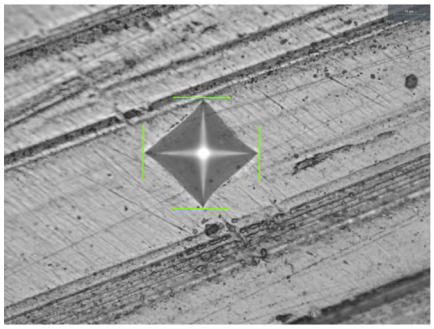

10 265 HV 0.2 0.04 0.04

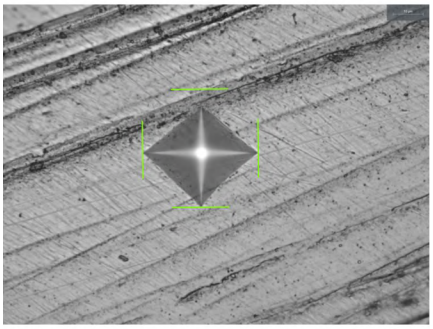

11 252 HV 0.2 0.04 0.04

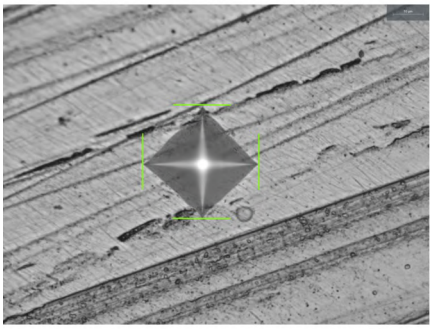

12 261 HV 0.2 0.04 0.04

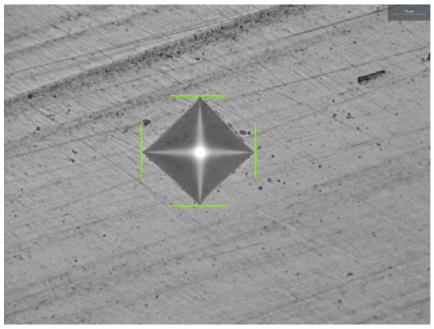

13 274 HV 0.2 0.04 0.04

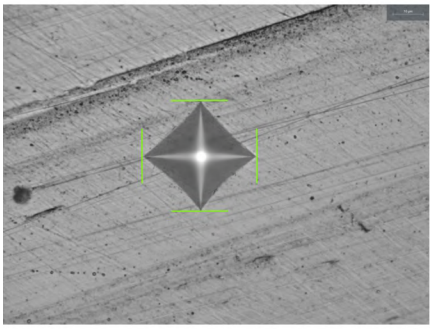

14 271 HV 0.2 0.04 0.04

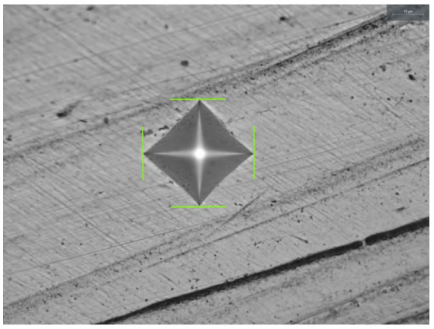

15 287 HV 0.2 0.04 0.04

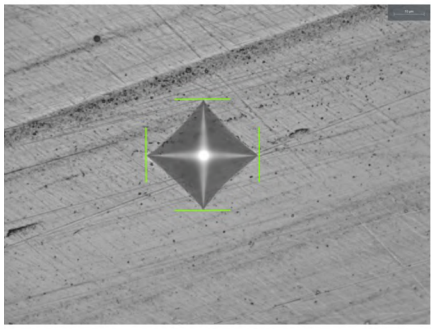

16 274 HV 0.2 0.04 0.04

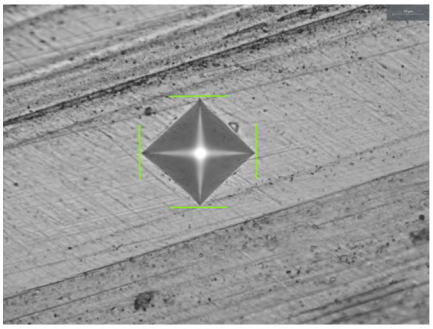

17 266 HV 0.2 0.04 0.04

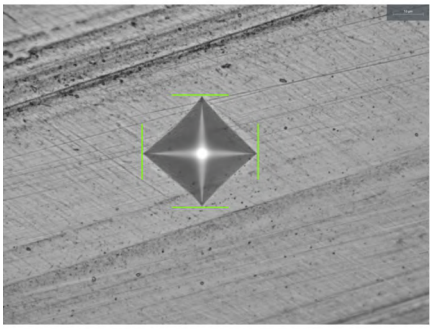

18 264 HV 0.2 0.04 0.04

Test point images:

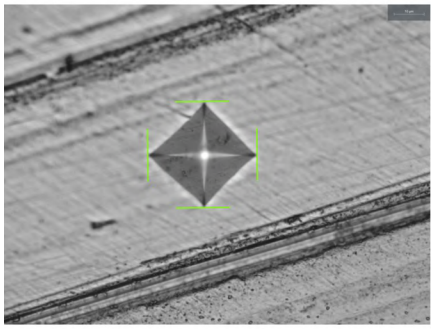

19 297 HV 0.2 0.04 0.03

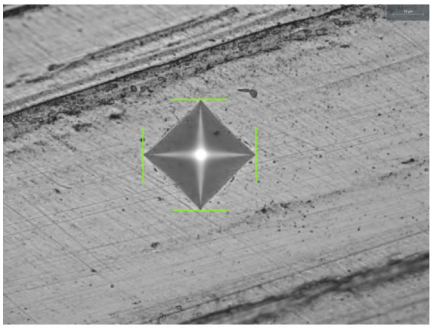

20 275 HV 0.2 0.04 0.04

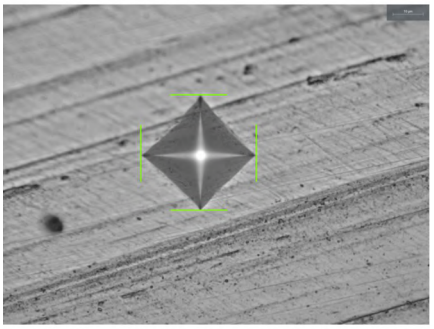

21 258 HV 0.2 0.04 0.04

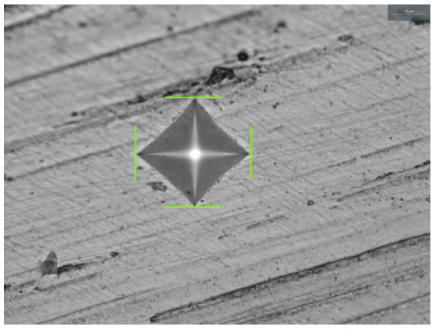

22 273 HV 0.2 0.04 0.04

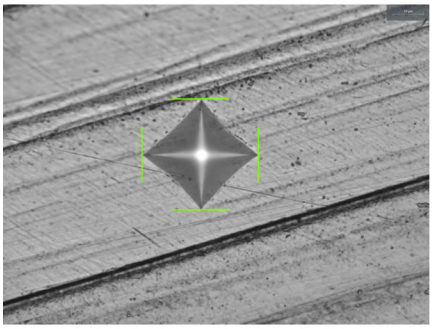

23 266 HV 0.2 0.04 0.04

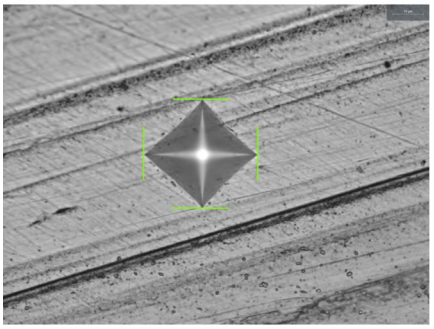

24 277 HV 0.2 0.04 0.04

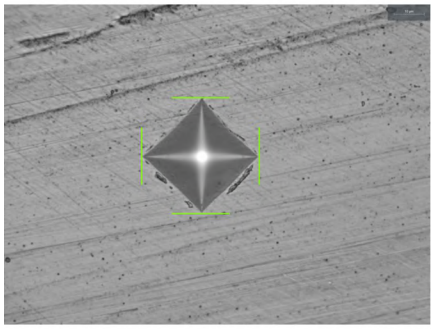

25 253 HV 0.2 0.04 0.04

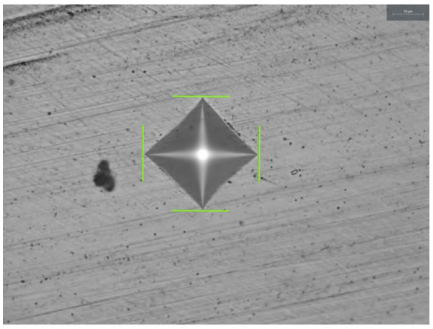

26 259 HV 0.2 0.04 0.04

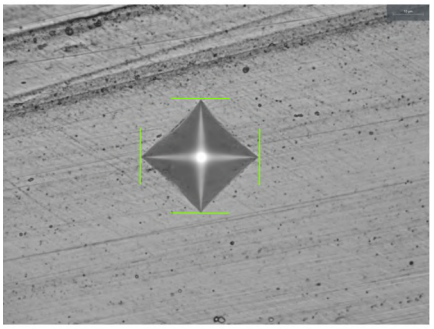

27 252 HV 0.2 0.04 0.04

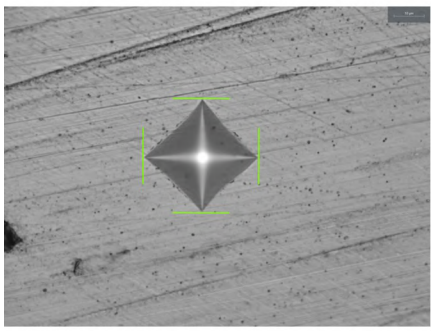

28 260 HV 0.2 0.04 0.04

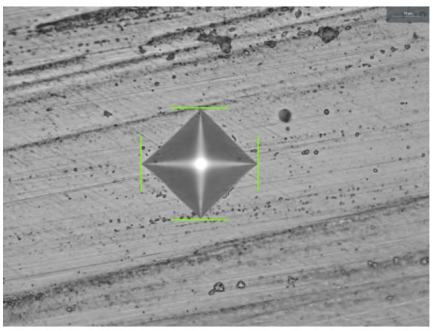

29 262 HV 0.2 0.04 0.04

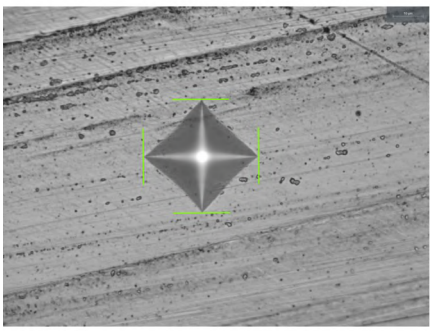

30 263 HV 0.2 0.04 0.04

Test point images:

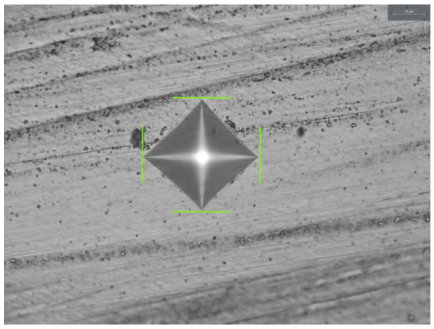

31 256 HV 0.2 0.04 0.04

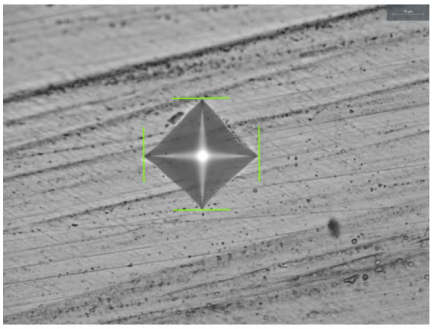

32 267 HV 0.2 0.04 0.04

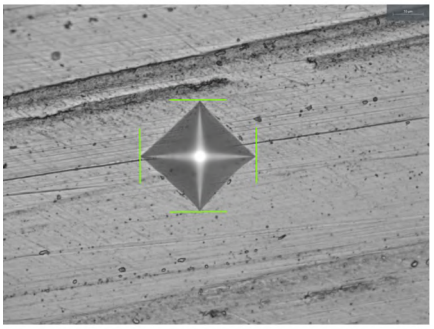

33 264 HV 0.2 0.04 0.04

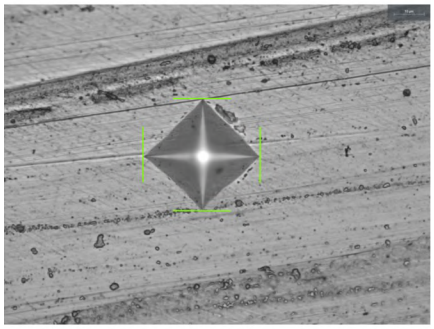

34 262 HV 0.2 0.04 0.04

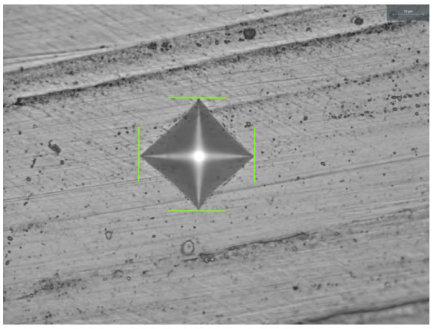

35 263 HV 0.2 0.04 0.04

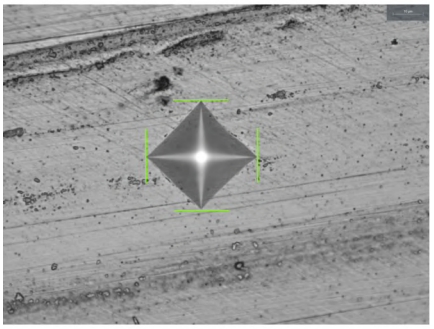

36 279 HV 0.2 0.04 0.04

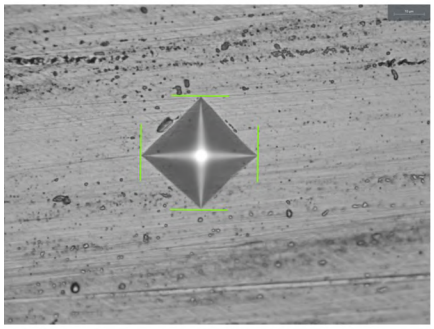

37 258 HV 0.2 0.04 0.04

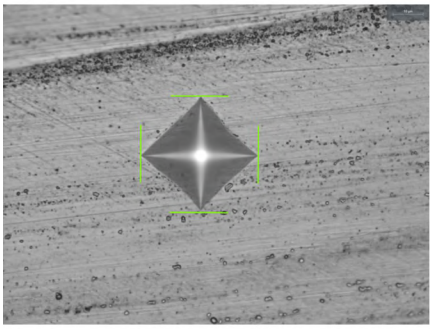

38 251 HV 0.2 0.04 0.04

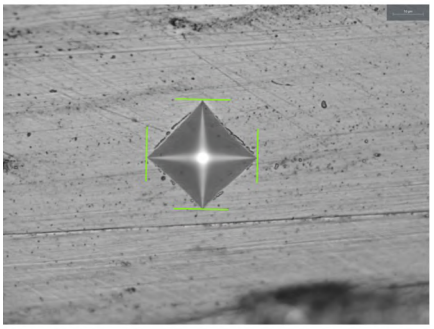

39 283 HV 0.2 0.04 0.04

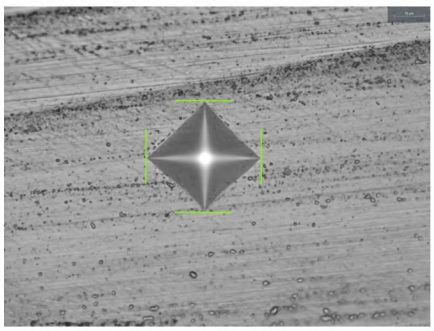

40 267 HV 0.2 0.04 0.04

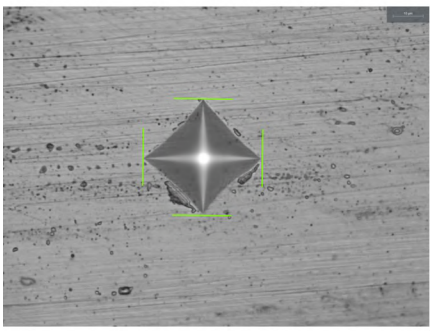

41 247 HV 0.2 0.04 0.04

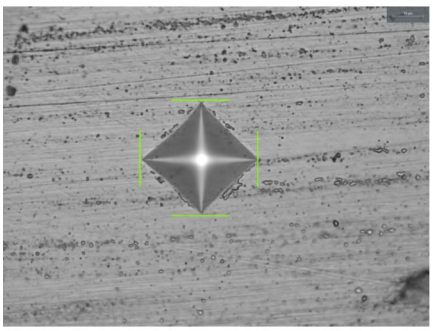

42 253 HV 0.2 0.04 0.04

Testing report

Test point images:

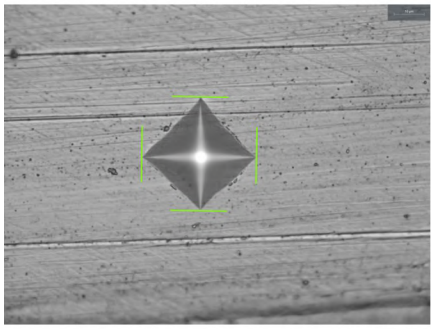

43 263 HV 0.2 0.04 0.04

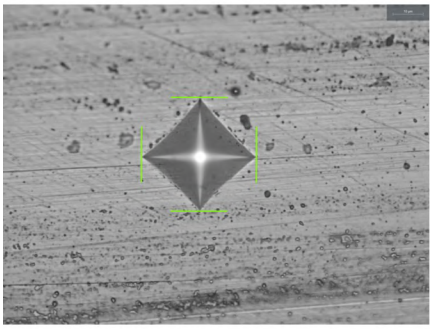

44 263 HV 0.2 0.04 0.04

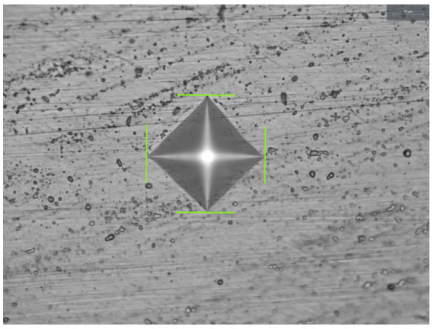

45 247 HV 0.2 0.04 0.04

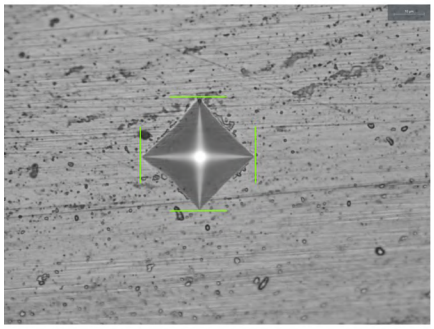

46 262 HV 0.2 0.04 0.04

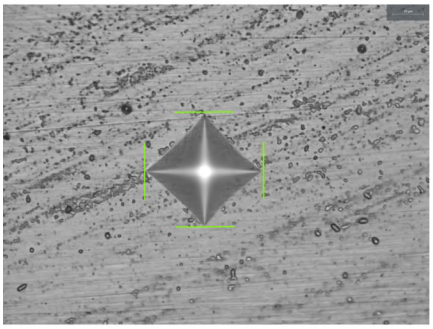

47 252 HV 0.2 0.04 0.04

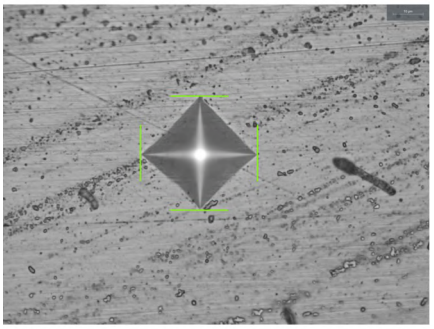

48 258 HV 0.2 0.04 0.04

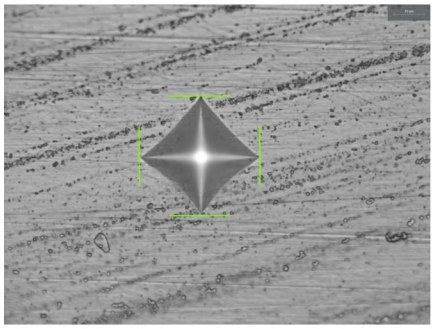

49 238 HV 0.2 0.04 0.04

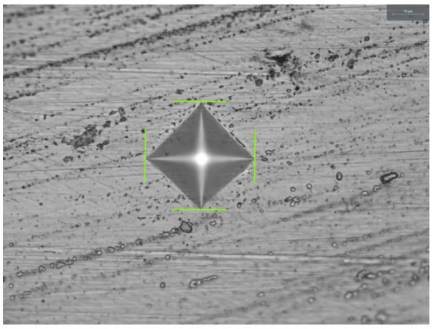

50 291 HV 0.2 0.04 0.04

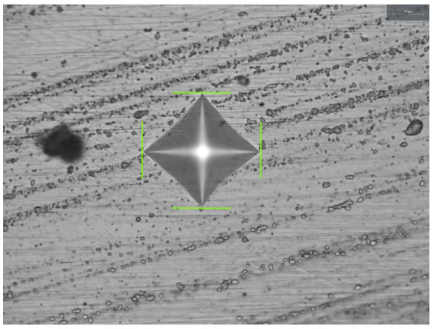

51 251 HV 0.2 0.04 0.04

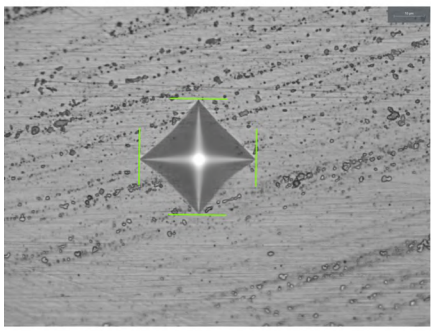

52 253 HV 0.2 0.04 0.04

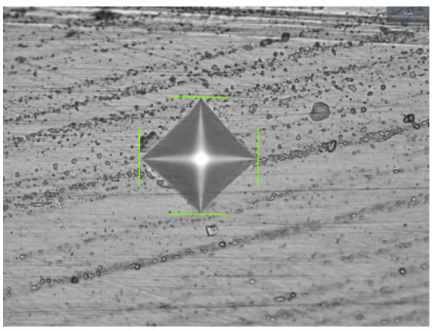

53 248 HV 0.2 0.04 0.04

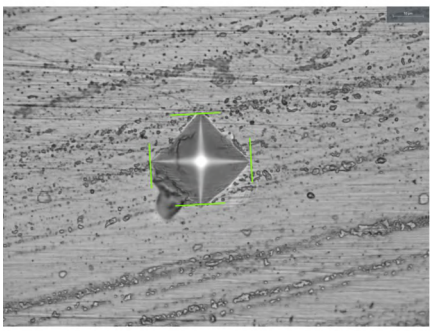

54 377 HV 0.2 0.03 0.03

Test point images:

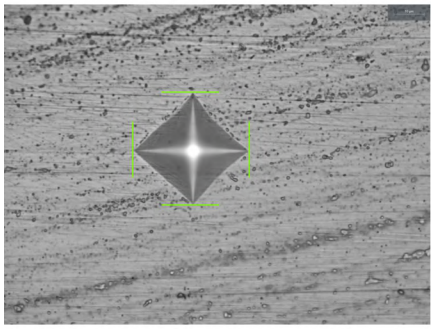

55 262 HV 0.2 0.04 0.04

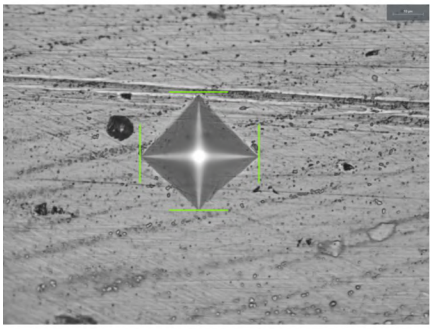

56 245 HV 0.2 0.04 0.04

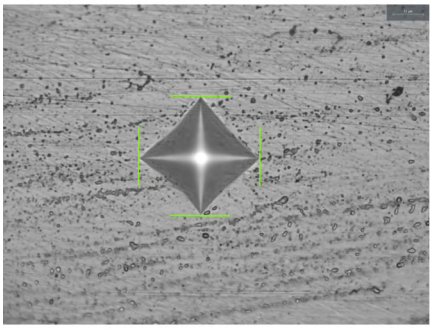

57 237 HV 0.2 0.04 0.04

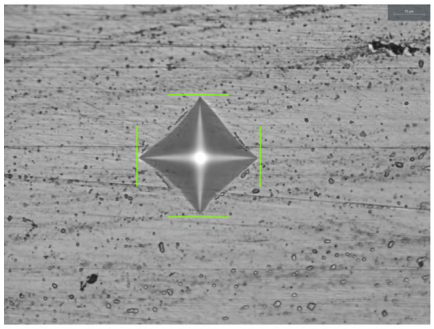

58 228 HV 0.2 0.04 0.04

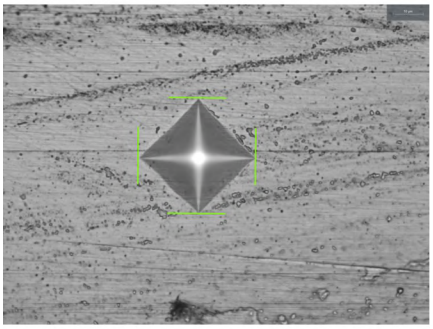

59 253 HV 0.2 0.04 0.04

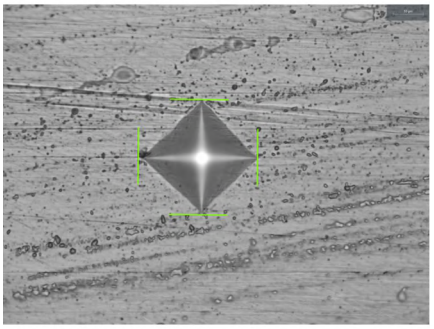

60 250 HV 0.2 0.04 0.04

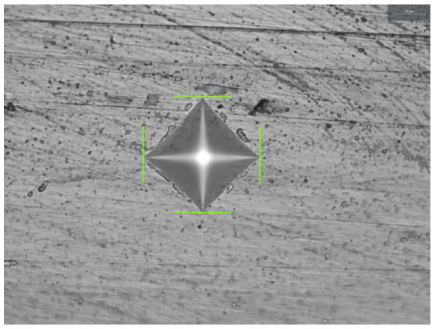

61 253 HV 0.2 0.04 0.04

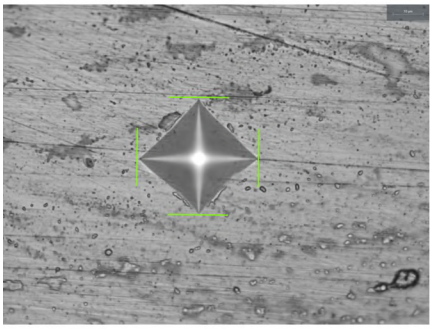

62 241 HV 0.2 0.04 0.04

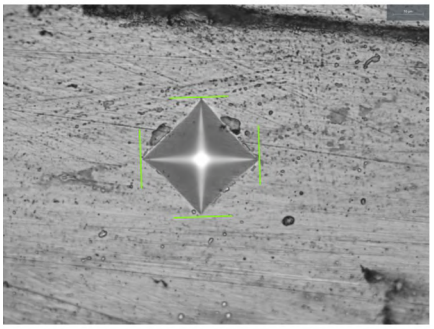

63 242 HV 0.2 0.04 0.04

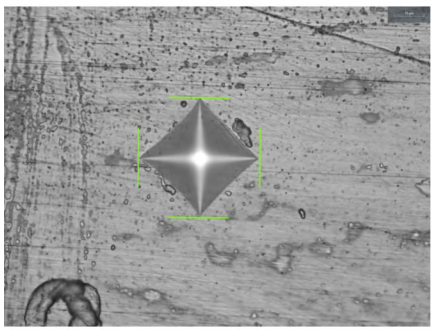

64 236 HV 0.2 0.04 0.04

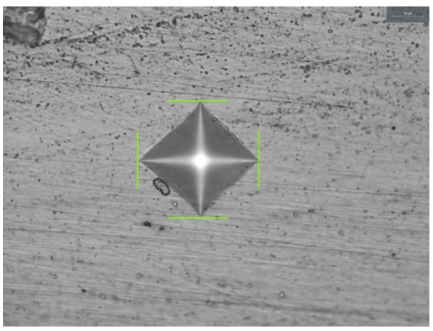

65 242 HV 0.2 0.04 0.04

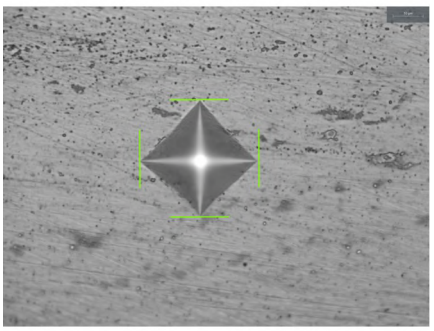

66 247 HV 0.2 0.04 0.04

Test point images:

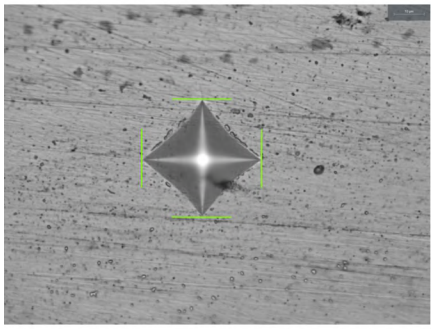

67 243 HV 0.2 0.04 0.04

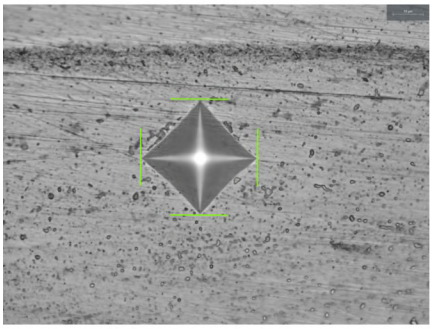

68 253 HV 0.2 0.04 0.04

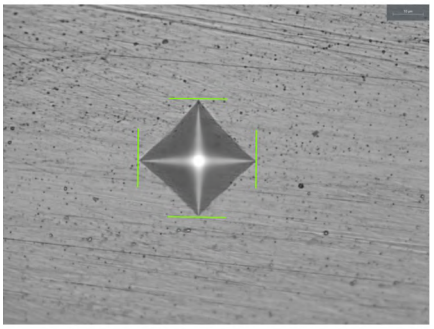

69 246 HV 0.2 0.04 0.04

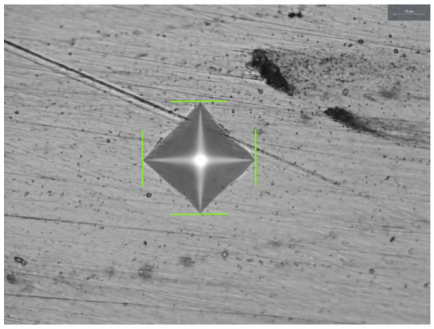

70 270 HV 0.2 0.04 0.04

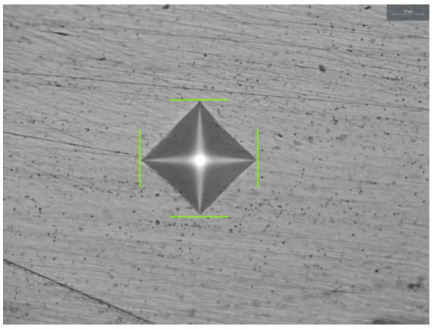

71 249 HV 0.2 0.04 0.04

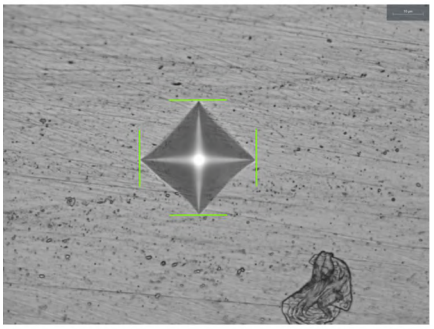

72 256 HV 0.2 0.04 0.04

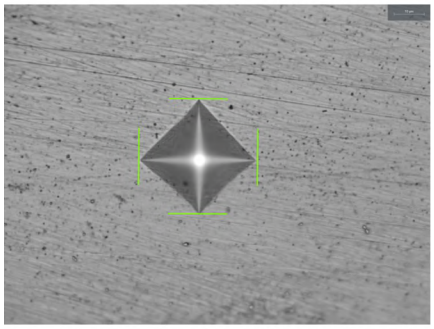

73 252 HV 0.2 0.04 0.04

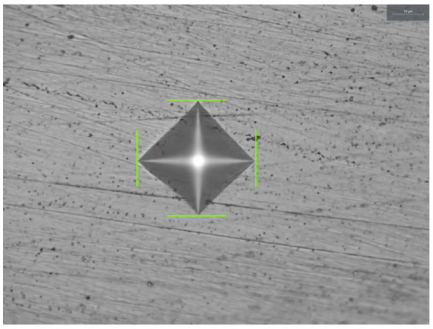

74 251 HV 0.2 0.04 0.04

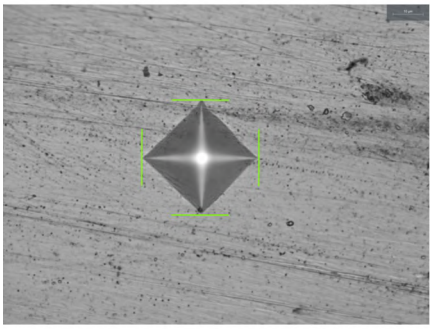

75 256 HV 0.2 0.04 0.04

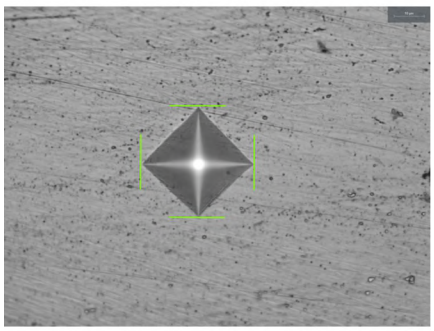

76 272 HV 0.2 0.04 0.04

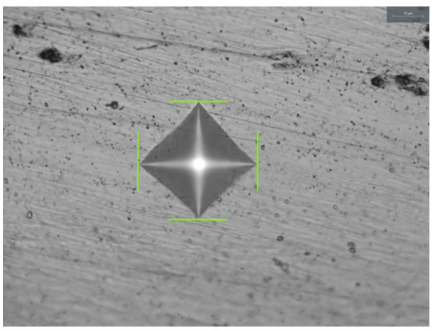

77 243 HV 0.2 0.04 0.04

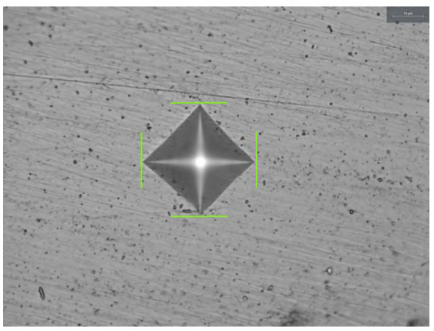

78 263 HV 0.2 0.04 0.04

Test point images:

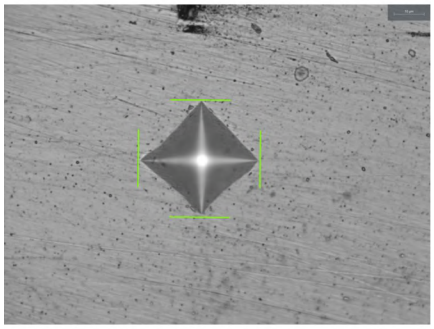

79 241 HV 0.2 0.04 0.04

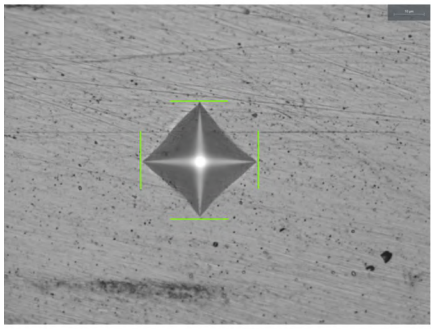

80 248 HV 0.2 0.04 0.04

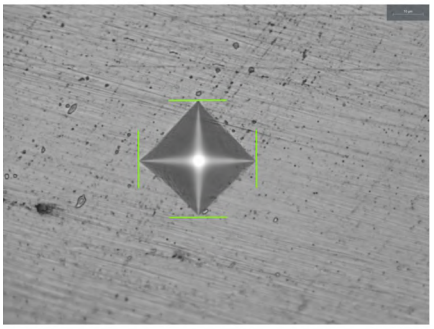

81 250 HV 0.2 0.04 0.04

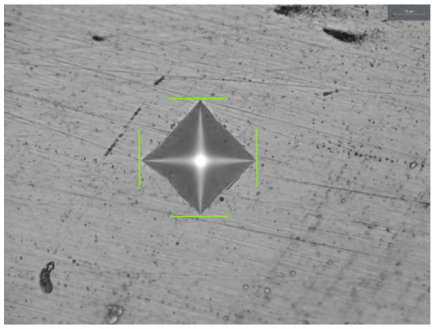

82 248 HV 0.2 0.04 0.04

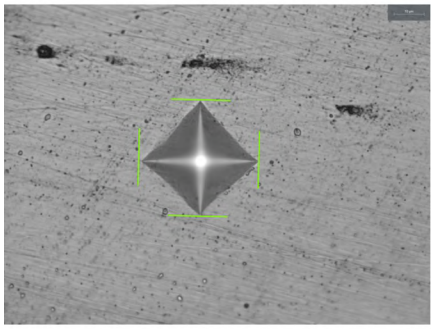

83 246 HV 0.2 0.04 0.04

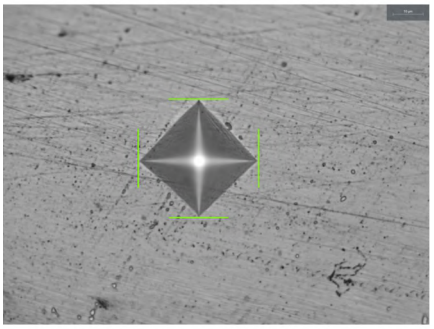

84 242 HV 0.2 0.04 0.04

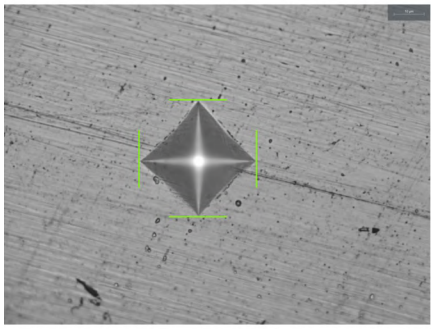

85 251 HV 0.2 0.04 0.04

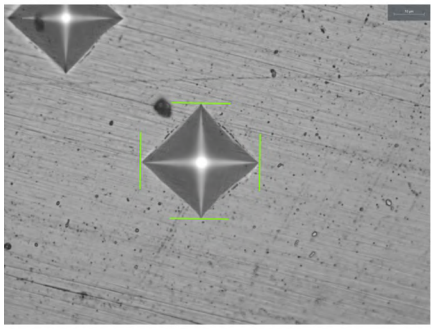

86 249 HV 0.2 0.04 0.04

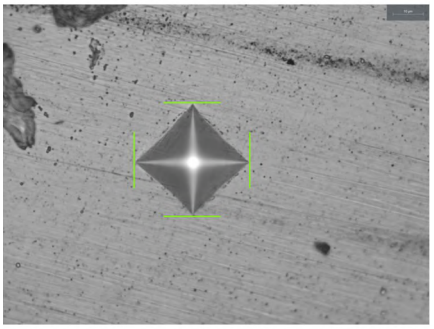

87 262 HV 0.2 0.04 0.04

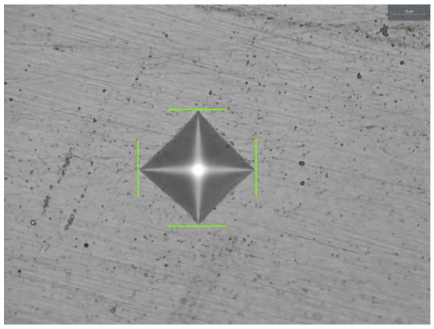

88 250 HV 0.2 0.04 0.04

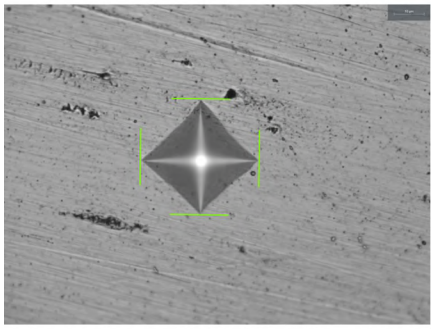

89 250 HV 0.2 0.04 0.04

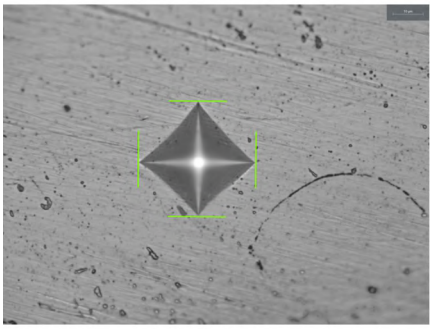

90 253 HV 0.2 0.04 0.04

Test point images:

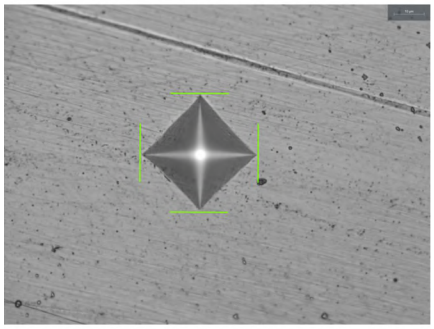

91 245 HV 0.2 0.04 0.04

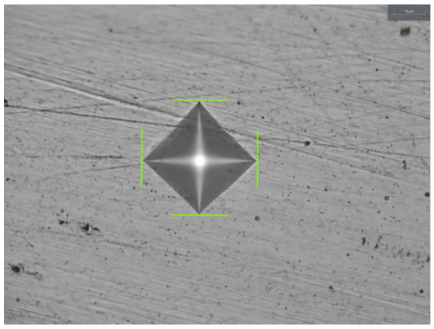

92 259 HV 0.2 0.04 0.04

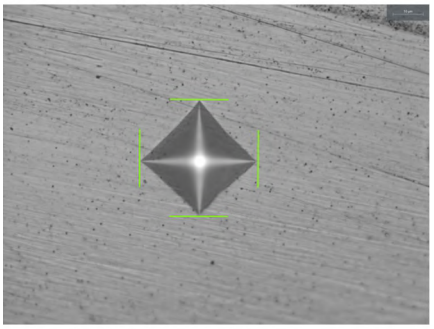

93 248 HV 0.2 0.04 0.04

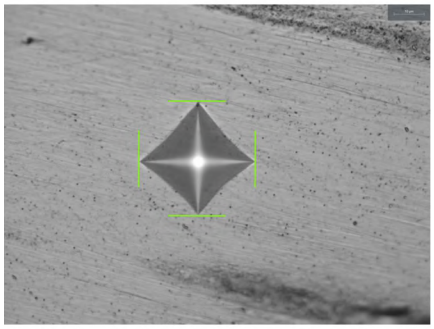

94 258 HV 0.2 0.04 0.04

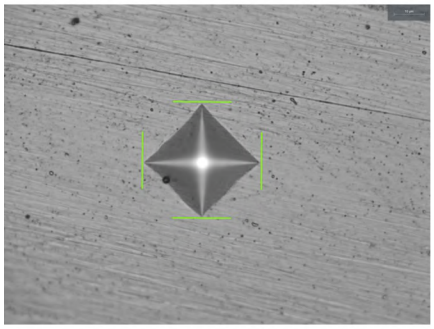

95 248 HV 0.2 0.04 0.04

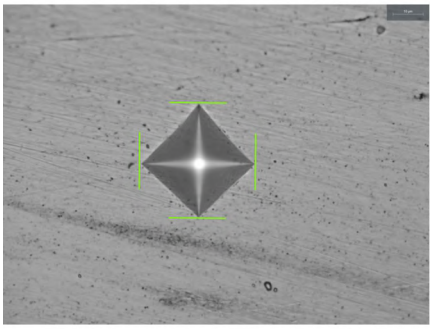

96 257 HV 0.2 0.04 0.04

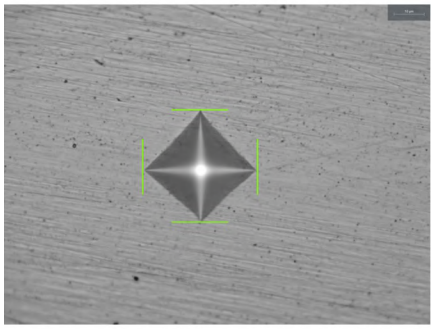

97 267 HV 0.2 0.04 0.04

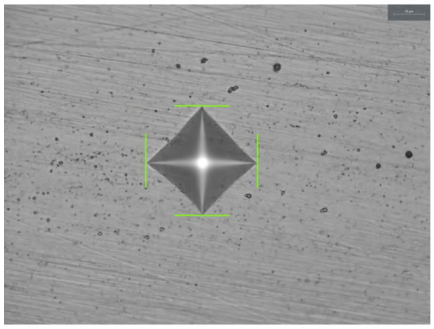

98 281 HV 0.2 0.04 0.04

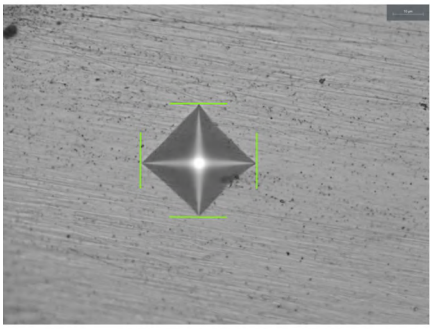

99 260 HV 0.2 0.04 0.04

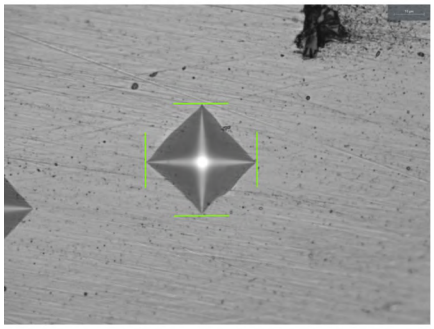

100 275 HV 0.2 0.04 0.04

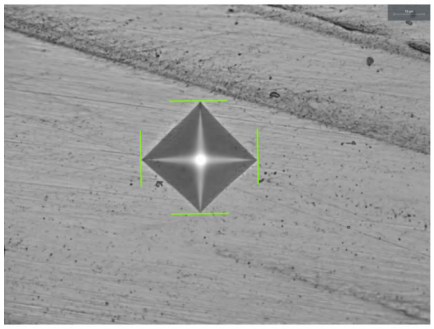

101 260 HV 0.2 0.04 0.04

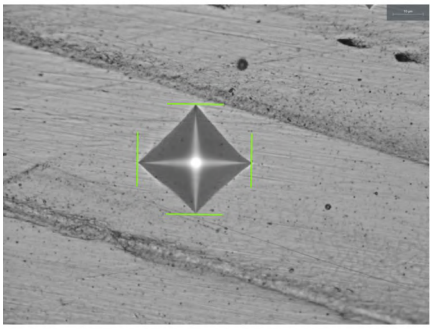

102 274 HV 0.2 0.04 0.04

Test point images:

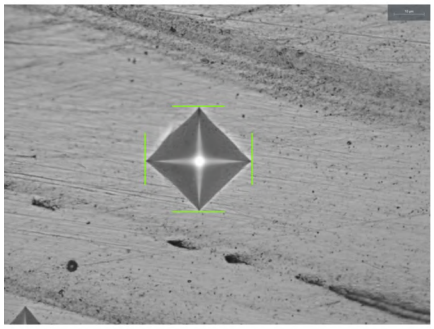

103 305 HV 0.2 0.04 0.03

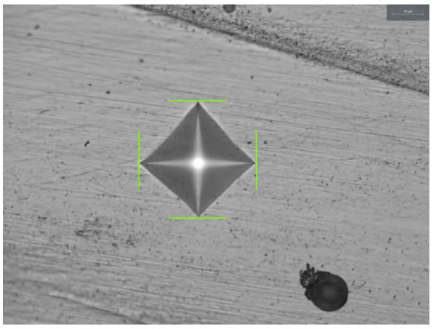

104 250 HV 0.2 0.04 0.04

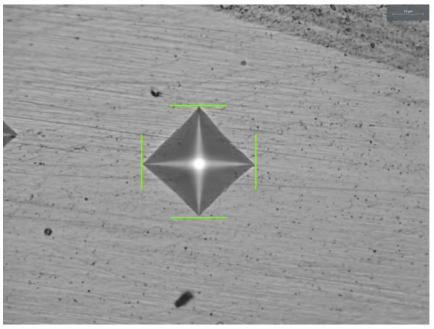

105 270 HV 0.2 0.04 0.04

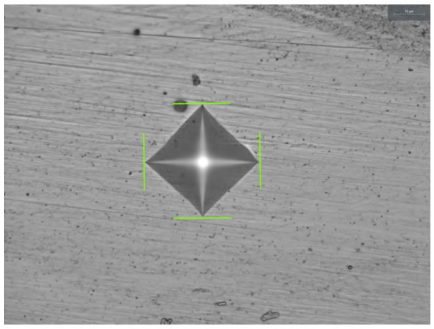

106 259 HV 0.2 0.04 0.04

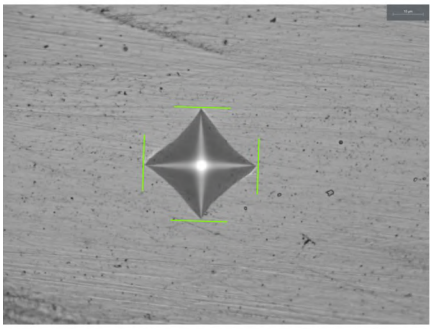

107 264 HV 0.2 0.04 0.04

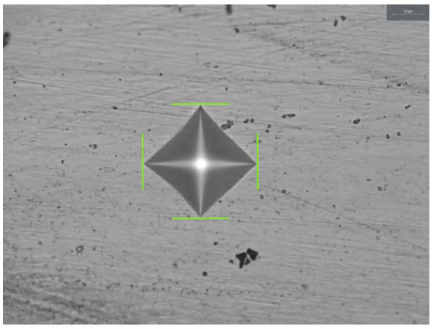

108 262 HV 0.2 0.04 0.04

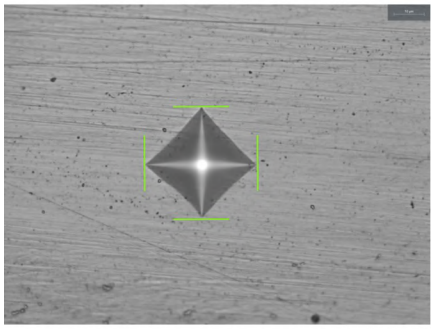

109 271 HV 0.2 0.04 0.04

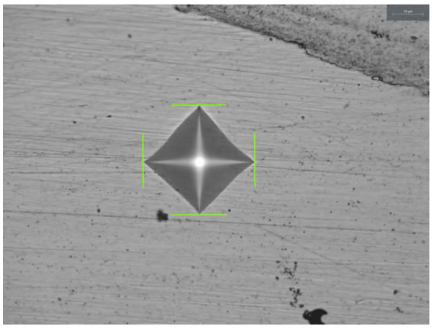

110 281 HV 0.2 0.04 0.04

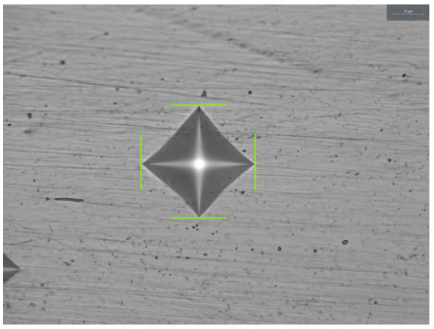

111 267 HV 0.2 0.04 0.04

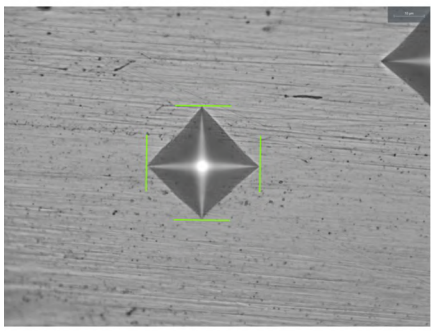

112 265 HV 0.2 0.04 0.04

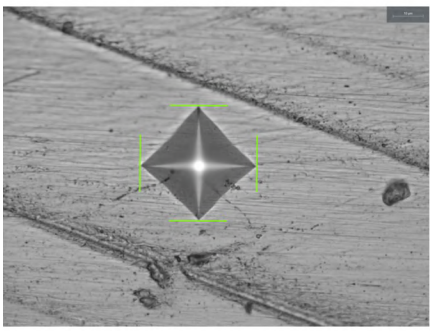

113 256 HV 0.2 0.04 0.04

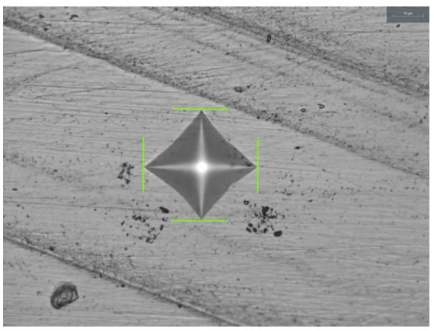

114 270 HV 0.2 0.04 0.04

Testing report

Test point images:

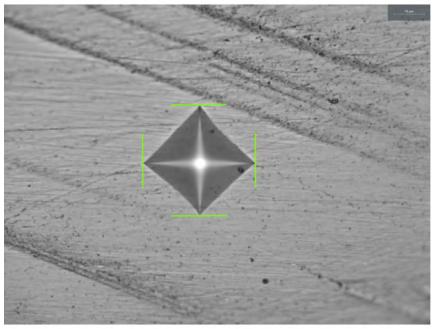

115 275 HV 0.2 0.04 0.04

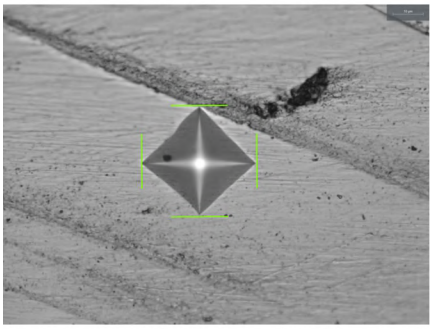

116 269 HV 0.2 0.04 0.04

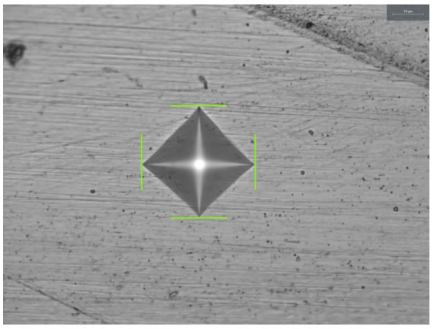

117 270 HV 0.2 0.04 0.04

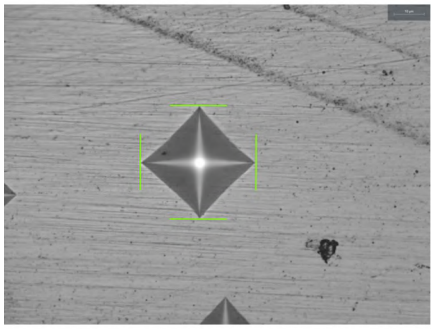

118 262 HV 0.2 0.04 0.04

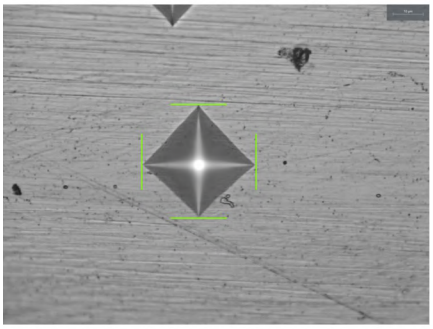

119 265 HV 0.2 0.04 0.04

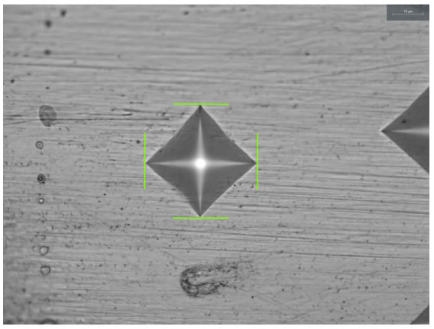

120 268 HV 0.2 0.04 0.04

Signature:

5.6 Dilution zone measurements

In here, the measurements of the dilution zone are shown. They were taken in the 40% power level test sample, for the different levels of overlapping.

	40PL						
	Single Tracks			0% OL	15% OL	30% OL	40% OL
	Track 1	Track 2	Track 3				
Mean	0,0135	0,020111111	0,012375	0,013628205	0,011716418	0,012431373	0,012636364
Deviation	0,002881	0,022591173	0,004534	0,004521547	0,003204192	0,003705428	0,002965624
	Measures [mm]	Measures [mm]	Measures [mm]	Measures [mm]	Measures [mm]	Measures [mm]	Measures [mm]
	0,015	0,014	0,013	0,016	0,006	0,008	0,011
	0,018	0,012	0,019	0,012	0,009	0,009	0,017
	0,011	0,009	0,011	0,012	0,021	0,008	0,013
	0,013	0,012	0,009	0,012	0,015	0,024	0,009
	0,014	0,011	0,012	0,011	0,014	0,025	0,013
	0,01	0,012	0,012	0,01	0,015	0,014	0,011
		0,018	0,018	0,015	0,013	0,012	0,011
		0,013	0,005	0,012	0,016	0,011	0,012
		0,08		0,013	0,01	0,011	0,015
				0,013	0,009	0,014	0,016
				0,017	0,018	0,013	0,01
				0,017	0,016	0,011	0,016
				0,014	0,013	0,01	0,014
				0,013	0,012	0,017	0,01
				0,011	0,008	0,011	0,009
				0,012	0,012	0,011	0,012
				0,01	0,015	0,014	0,015
				0,009	0,009	0,012	0,012
				0,012	0,009	0,011	0,013
				0,027	0,011	0,011	0,012
				0,017	0,012	0,01	0,015
				0,011	0,009	0,009	0,016
				0,012	0,01	0,009	0,017
				0,012	0,01	0,012	0,013
				0,015	0,008	0,015	0,013
				0,019	0,009	0,015	0,014
				0,023	0,01	0,014	0,011
				0,021	0,01	0,015	0,012
				0,021	0,014	0,012	0,01
				0,009	0,012	0,008	0,009
				0,01	0,009	0,012	0,01
				0,018	0,012	0,013	0,013
				0,013	0,011	0,012	0,011
				0,01	0,013	0,01	0,018
				0,012	0,013	0,012	0,011
				0,011	0,013	0,008	0,014
				0,017	0,015	0,018	0,009
				0,025	0,013	0,01	0,021
				0,01	0,013	0,013	0,011
				0,008	0,01	0,014	0,013
				0,01	0,011	0,01	0,011

				0,024	0,008	0,011	0,005
				0,013	0,016	0,011	0,017
				0,022	0,019	0,011	0,011
				0,011	0,009	0,019	
				0,01	0,014	0,013	
				0,015	0,015	0,005	
				0,021	0,014	0,011	
				0,012	0,012	0,013	
				0,015	0,013	0,013	
				0,015	0,012	0,019	
				0,023	0,009		
				0,009	0,01		
				0,009	0,005		
				0,01	0,009		
				0,007	0,015		
				0,014	0,016		
				0,013	0,018		
				0,011	0,011		
				0,01	0,009		
				0,008	0,008		
				0,012	0,008		
				0,014	0,009		
				0,014	0,011		
				0,015	0,011		
				0,01	0,008		
				0,01	0,008		
				0,008			
				0,009			
				0,015			
				0,008			
				0,009			
				0,011			
				0,016			
				0,016			
				0,023			
				0,017			
				0,012			

Bibliography

[1] The World Material. "SS 304 Stainless Steel Properties, Tensile Yield Strength, Magnetic, Hardness". In: (). URL: https://www.theworldmaterial.com/type-304-grade-stainless-steel/.

[2] Oerlikon Metco. "Material Product Data Sheet Type 316L Austenitic Stainless Steel Powders for Additive Manufacturing". In: (). URL: https://www.oerlikon.com/ecoma/files/DSM-0272.0_AM_316L-AusteniticSteel.pdf?download=true.

[3] ASM International Handbook Committee. *ASM Handbook, Volume 06 - Welding, Brazing, and Soldering*. ASM International, pp. 588–592. ISBN: 978-1-61503-133-7.

[4] Minlin Zhong and W Liu. "Laser surface cladding: the state of the art and challenges. Proc Inst Mech Eng Part C: J Mech Eng Sci". In: *Proceedings of The Institution of Mechanical Engineers Part C-journal of Mechanical Engineering Science - PROC INST MECH ENG C-J MECH E* 224 (May 2010), pp. 1041–1060. DOI: 10.1243/09544062JMES1782.

[5] Dariusz Bartkowski et al. "Influence of Laser Cladding Parameters on Microstructure, Microhardness, Chemical Composition, Wear and Corrosion Resistance of Fe–B Composite Coatings Reinforced with B4C and Si Particles". In: *Coatings* 10.9 (2020). ISSN: 2079-6412. DOI: 10.3390/coatings10090809. URL: https://www.mdpi.com/2079-6412/10/9/809.

[6] Núria Martín and Carmen Arribas Arribas. *Ciencia de materiales para ingenieros*. Madrid: Pearson Educación, D.L. 2012. ISBN: 9788483227190.

[7] Núria Martín. *Materiales Estructurales para Sistemas Propulsivos (PA), Guiones*. Madrid, D.L. 2014.

[8] F. Mohs. *Treatise on Mineralogy: Or, The Natural History of the Mineral Kingdom*. Landmarks of science v. 1. A. Constable and Company, 1825. URL: https://books.google.ro/books?id=BpBFAAAAIAAJ.

[9] Buehler. "Buehler - Cosumables Calatogue". In: (). URL: http://www.trimid.rs/upload/documents/buhler/Buehler%20-%20Consumables.pdf.

[10] Struers. "MULTIFAST Safety Data Sheet". In: (). URL: https://www.struers.com/-/media/Library/SDS/United-States/Mounting/SDS-MULTIFAST-Black-US-EN-M0198.pdf.

[11] ASM International. "E384 17 - Standard Test Method for Microindentation Hardness of Materials1 Block-on-Ring Wear Test". In: ().